

Determination of new coefficients in the angular momentum and energy fluxes at infinity to 9PN for eccentric Schwarzschild extreme-mass-ratio inspirals using mode-by-mode fitting

Christopher Munna,¹ Charles R. Evans,¹ Seth Hopper,² and Erik Forseth³

¹*Department of Physics and Astronomy, University of North Carolina, Chapel Hill, North Carolina 27599, USA*

²*Department of Physics and Astronomy, Earlham College, Richmond, IN 47374, USA*

³*Graham Capital Management, Rowayton, CT 06853, USA*

We present an extension of work in an earlier paper showing high precision comparisons between black hole perturbation theory and post-Newtonian (PN) theory in their region of overlapping validity for bound, eccentric-orbit, Schwarzschild extreme-mass-ratio inspirals. As before we apply a numerical fitting scheme to extract eccentricity coefficients in the PN expansion of the gravitational wave fluxes, which are then converted to exact analytic form using an integer-relation algorithm. In this work, however, we fit to individual lmn modes to exploit simplifying factorizations that lie therein. Since the previous paper focused solely on the energy flux, here we concentrate initially on analyzing the angular momentum flux to infinity. A first step involves finding convenient forms for hereditary contributions to the flux at low-PN order, analogous to similar terms worked out previously for the energy flux. We then apply the upgraded techniques to find new PN terms through 9PN order and (at many PN orders) to e^{30} in the power series in eccentricity. With the new approach applied to angular momentum fluxes, we return to the energy fluxes at infinity to extend those previous results. Like before, the underlying method uses a MATHEMATICA code based on use of the Mano-Suzuki-Takasugi (MST) function expansion formalism to represent gravitational perturbations and spectral source integration (SSI) to find numerical results at arbitrarily high precision.

PACS numbers: 04.25.dg, 04.30.-w, 04.25.Nx, 04.30.Db

I. INTRODUCTION

At present the two-body problem is the subject of ongoing investigation in gravitational physics [1]. As two massive objects orbit one another, gravitational waves are emitted that carry off energy and angular momentum and drive an inspiral and eventual merger of the binary. Of particular interest is the class of binaries known as extreme-mass-ratio inspirals (EMRIs), in which the primary black hole of mass M is much heavier than the secondary compact object of mass μ (i.e., $\mu/M \ll 1$) [2]. Such systems will be sources of gravitational waves observable by the LISA detector set to launch in 2034 [3, 4]. EMRIs can be understood using black hole perturbation theory (BHPT), i.e., expansion in powers of the small mass ratio, and subsequent calculation of the gravitational self-force (GSF) [5].

An orthogonal approach for approximating the motion of binary orbits is post-Newtonian (PN) theory [6], which is most suited for widely separated orbits or, equivalently, slowly-orbiting systems. In PN theory corrections are computed in powers of the small velocity $v/c \ll 1$. Additionally, a fruitful region of overlap exists between BHPT and PN regimes, where simultaneously $\mu/M \ll 1$ and $v/c \ll 1$ and where both formalisms may be applied and compared [7–26].

Some of these BHPT studies have involved application of the MST (for Mano, Suzuki, and Takasugi) formalism [27, 28] for obtaining homogeneous solutions to the radial Teukolsky equation. In [29], the authors used the MST formalism, along with a PN expansion of the

geodesic equation, to develop PN expansions for the rates of change of the constants of motion for arbitrarily inclined, eccentric orbits on Kerr backgrounds. That work was recently extended in [20], producing results accurate to 4PN order relative to the Newtonian result and accurate to $\mathcal{O}(e^6)$ in a power series expansion in the orbital eccentricity. Others [12, 14, 15, 30] applied MST to arrive at extremely high-order PN expansions for the rates of change of orbital constants as well as self-force quantities in the case of circular orbits on both Schwarzschild and Kerr backgrounds.

In an earlier paper [21] (hereafter referred to as Paper I), several of us extended the methods of [14, 15, 17] to compute the energy flux radiated to infinity by eccentric EMRIs on Schwarzschild backgrounds, using the method of spectral source integration [31] to treat the eccentric source. By using a MATHEMATICA code and computing the flux to high precision (up to 200 significant digits) for a variety of orbital parameters, it proved possible to fit out multiple terms in the high-order PN expansion (to 7PN relative order) to varying depths in the power series expansion in eccentricity e . Furthermore, by applying experimental mathematics techniques [17] such as the PSLQ algorithm [32] (an integer-relation algorithm), it was possible to determine exact, analytic forms for a number of those expansion coefficients.

In the present paper, we take those methods a step further by performing a separate fit on each individual lmn mode. Past work [33] revealed that for circular orbits the lm modes of the energy flux have patterns in the PN expansion that allow factorization and simplification,

which in turn helps improve the numerical fit. Motivated by those discoveries in circular orbits, we found similar, generalized simplifications and factorizations in the lmn modes for eccentric orbits, which also allows sharply improved fitting. With these techniques, we are able to push the analytical understanding of the gravitational wave fluxes to 9PN order and to as far as $\mathcal{O}(e^{30})$ in eccentricity for most PN terms. At some PN orders it has been possible [26, 34] to develop an underlying physical explanation for the high PN order flux contributions in terms of lower order multipole moments of the source motion.

The first application we make of this new technique is to gravitational wave angular momentum emission to infinity. Most of the prior understanding of angular momentum emission in eccentric EMRIs, out to 3PN relative order, is found in [35], which extended comparable analysis on energy fluxes found in [36, 37]. Beyond that, as noted above, Sago and Fujita [20] showed expansions for the angular momentum flux to 4PN relative order through $\mathcal{O}(e^6)$ in the eccentricity expansion. As part of our analysis, we verify all of these previous results. We then apply the new approach to take a renewed look at the energy fluxes, and present an improved determination of that expansion that augments the results found in Paper I.

The outline of this paper is as follows. We start in Sec. II by briefly reviewing the MST and SSI methods that are used to calculate the first order gravitational field perturbation and thence the first-order-in-mass-ratio angular momentum and energy fluxes. In Sec. III we review the current state of knowledge on the fluxes as determined by PN theory. We continue in that section with further investigation of the angular momentum flux finding original arbitrary-order expansions of the low-PN order enhancement functions via decomposition into Fourier modes. Like the corresponding section in Paper I (Sec. IV), we focus on the hereditary or “tail” terms, briefly deriving their asymptotic forms to verify the eccentricity singular behavior as $e \rightarrow 1$. We then in Sec. IV detail the improved method of fitting by lmn mode, which involves the use of a novel eccentric-orbit analog of the well-known “eulerlog” function [33, 38]. Finally, in Secs. V and VI we present the new coefficients we have found using this method, first giving angular momentum flux terms through 9PN order (some of these angular momentum flux terms were found earlier by the methods of Paper I and reported in [39]) and then updating the energy flux results of Paper I to the same level. The now-known length of many of these expressions precludes giving them fully in this paper. Though where we have truncated expressions for brevity in Secs. V and VI, the full results can be found in a MATHEMATICA notebook posted on the archival Black Hole Perturbation Toolkit website [40].

Throughout this paper we use units in which $c = G = 1$ and metric signature $(- + +)$. Our notation for the RWZ formalism follows that found in Paper I, which in

part derives from notational changes for tensor spherical harmonics and perturbation amplitudes made by Martel and Poisson [41]. For the MST formalism, we largely make use of the discussion and notation found in the review by Sasaki and Tagoshi [42].

II. BHPT BACKGROUND AND FORMALISM

The angular momentum and energy radiated to infinity by a small body in eccentric orbit about a Schwarzschild black hole can be described using the methods of first-order BHPT. At this order the small body can be treated as a point mass. In this section we briefly summarize the notation used for describing bound eccentric orbits and review the formalism behind our flux calculations. Full details can be found in Paper I.

A. Bound orbits on a Schwarzschild background

We consider generic bound motion of a point mass μ around a Schwarzschild black hole of mass M in the equatorial plane, with $\mu/M \ll 1$. At lowest order in the mass ratio the primary can be regarded as a stationary black hole. Schwarzschild coordinates $x^\mu = (t, r, \theta, \varphi)$ are used, with the line element given by

$$ds^2 = -f dt^2 + f^{-1} dr^2 + r^2 (d\theta^2 + \sin^2 \theta d\varphi^2), \quad (2.1)$$

where $f(r) = 1 - 2M/r$. Likewise at lowest order, the motion of the small body will approximate that of a geodesic in this background. Several first integrals can be exploited allowing the four-velocity to be written as

$$u^\alpha(\tau) = \frac{dx_p^\alpha(\tau)}{d\tau} = \left(\frac{\mathcal{E}}{f_p}, u^r, 0, \frac{\mathcal{L}}{r_p^2} \right), \quad (2.2)$$

where \mathcal{E} is the specific energy, \mathcal{L} is the angular momentum, and the subscript p indicates evaluation at the location of the particle. The radial motion is given by

$$\dot{r}_p^2(t) = f_p^2 \left[1 - \frac{f_p}{\mathcal{E}^2} \left(1 + \frac{\mathcal{L}^2}{r_p^2} \right) \right], \quad (2.3)$$

where dot refers to a derivative with respect to coordinate time t .

As usual, we reparameterize these equations using Darwin’s geometric quantities p (the semi-latus rectum) and e (the eccentricity) [43–45], which are more conducive to PN expansion. These parameters are related to \mathcal{E} and \mathcal{L} by

$$\mathcal{E}^2 = \frac{(p-2)^2 - 4e^2}{p(p-3-e^2)}, \quad \mathcal{L}^2 = \frac{p^2 M^2}{p-3-e^2}. \quad (2.4)$$

We transform similarly the curve parameter of the orbital motion from τ to Darwin’s relativistic anomaly χ , casting the radial position into the Keplerian-like form

$$r_p(\chi) = \frac{pM}{1 + e \cos \chi}, \quad (2.5)$$

where one radial libration corresponds to a 2π advance in χ [43]. This equation can be combined with previous ones to generate simple, singularity-free ordinary differential equations (ODEs) for each remaining Schwarzschild coordinate location [44]. In this way, $\varphi_p(\chi)$ can be integrated analytically in terms of elliptic functions and $t_p(\chi)$ can be determined numerically.

In addition, this representation provides simple means to compute the two fundamental frequencies, Ω_r and Ω_φ . Explicitly, the radial libration period is found to be

$$T_r = \int_0^{2\pi} \frac{r_p(\chi)^2}{M(p-2-2e\cos\chi)} \left[\frac{(p-2)^2 - 4e^2}{p-6-2e\cos\chi} \right]^{1/2} d\chi,$$

with $\Omega_r = 2\pi/T_r$. The frequency of (mean) azimuthal advance is

$$\Omega_\varphi = \frac{4}{T_r} \left(\frac{p}{p-6-2e} \right)^{1/2} K \left(-\frac{4e}{p-6-2e} \right), \quad (2.6)$$

where $K(m)$ is the complete elliptic integral of the first kind [46]. Finally, the compactness parameter y , which is the PN expansion parameter we use, is given by $y = (M\Omega_\varphi)^{2/3}$.

As the expressions above show, y is a function (through Ω_φ and T_r) of p and e . For a given p and e , it proved useful to compute y to 600 decimal places for the numerical fitting work in this paper. Such precision is straightforward to obtain because the integrand in the integral for T_r is periodic and smooth in χ , leading to exponential convergence in a Riemann sum (as summarized in [31]).

B. The RWZ master equation

The geodesic motion of the small body provides the source of a perturbation to the background Schwarzschild metric. Finding this perturbation is convenient in the Regge-Wheeler-Zerilli (RWZ) formalism, and for purposes of computing fluxes we need not go beyond calculating the master functions. In a spherical harmonic decomposition, for each l, m the master function satisfies a single inhomogeneous time domain (TD) equation of the form

$$\left[-\frac{\partial^2}{\partial t^2} + \frac{\partial^2}{\partial r_*^2} - V_l(r) \right] \Psi_{lm}(t, r) = S_{lm}(t, r). \quad (2.7)$$

Here $r_* = r + 2M \ln |r/2M - 1|$ is the tortoise coordinate and the source is a distribution of the form $S_{lm}(t, r) \equiv G_{lm}(t) \delta[r - r_p(t)] + F_{lm}(t) \delta'[r - r_p(t)]$. Both the source term and the potential $V_l(r)$ are $(l+m)$ parity-dependent.

While this equation can be solved directly in the TD (e.g. [47]), our method works in the frequency domain (FD) and utilizes the MST formalism to produce solutions at extremely high accuracy. Transforming the field and source to the FD involves Fourier series

$$\Psi_{lm}(t, r) = \sum_{n=-\infty}^{\infty} X_{lmn}(r) e^{-i\omega t}, \quad (2.8)$$

$$S_{lm}(t, r) = \sum_{n=-\infty}^{\infty} Z_{lmn}(r) e^{-i\omega t}, \quad (2.9)$$

since discrete frequencies $\omega \equiv \omega_{mn} = m\Omega_\varphi + n\Omega_r$ arise as part of the bi-periodicity of the bound motion.

In this way, the TD master equation is reduced in the FD to a set of inhomogeneous ODEs now tagged by harmonic n (from the eccentric motion) as well as spherical harmonic indices l, m ,

$$\left[\frac{d^2}{dr_*^2} + \omega^2 - V_l(r) \right] X_{lmn}(r) = Z_{lmn}(r). \quad (2.10)$$

The homogeneous version to this equation yields two independent solutions: X_{lmn}^- , with downgoing causal behavior at the horizon, and X_{lmn}^+ , with outgoing causal behavior at infinity.

It is possible to determine the homogeneous solution for the odd-parity master function using the MST formalism first, and then to recover the even-parity counterpart using the Detweiler-Chandrasekar transformation [48–51]. Though a direct MST formalism for the (odd-parity) RWZ functions X_{lmn}^- and X_{lmn}^+ exists [27], we instead computed the MST solutions to the related Bardeen-Press-Teukolsky equation [44, 52]. Then X_{lmn}^\pm are recovered using another version of the Detweiler-Chandrasekar transformation. We refer the reader to Paper I for details.

Once the RWZ functions are computed, the resulting X_{lmn}^\pm will not be unit normalized at infinity nor at the horizon, since the MST solution involves iterating a recurrence relation starting with an arbitrary value a_0 . We separately and precisely determine the resulting amplitudes at infinity and at the horizon and divide these off to produce unit-normalized functions

$$\hat{X}_{lmn}^\pm \sim e^{\pm i\omega r_*}, \quad r_* \rightarrow \pm\infty. \quad (2.11)$$

These unit-normalized homogeneous solutions are then used [53] in an integration over the source to determine the proper normalization amplitudes C_{lmn}^\pm , as we summarize next.

C. The TD solution $\Psi_{lm}(t, r)$ and the angular momentum flux

With the unit-normalized solutions computed, the TD function $\Psi_{lm}(t, r)$ can be directly constructed using the method of extended homogeneous solutions (EHS) [53, 54]. This process involves a pair of homogeneous solutions of the TD equation (2.7)

$$\Psi_{lm}^\pm(t, r) \equiv \sum_n C_{lmn}^\pm \hat{X}_{lmn}^\pm(r) e^{-i\omega t}, \quad r > 2M, \quad (2.12)$$

where C_{lmn}^\pm are the two key sets of normalization constants (determined below). The full (particular) solution

to the RWZ equation (2.7) is then formed by abutting the two TD EHS $\Psi^\pm(t, r)$ at the particle's location

$$\Psi_{lm}(t, r) = \Psi_{lm}^+(t, r)\theta[r - r_p(t)] + \Psi_{lm}^-(t, r)\theta[r_p(t) - r]. \quad (2.13)$$

Unlike the standard procedure of constructing a solution to (2.7) by summing the inhomogeneous FD solutions $X_{lmn}(r)$ of (2.10) (found by variation of parameters or equivalently use of the Green function), the EHS method experiences no Gibbs behavior near $r_p(t)$ nor within the radial libration region. Instead the sums in (2.12) converge exponentially for all r .

The only remaining issue is finding the particular values of C_{lmn}^\pm , equivalent to incorporating the internal boundary condition at the discontinuity at $r_p(t)$. As shown in [53], these coefficients are given by

$$C_{lmn}^\pm = \frac{1}{W_{lmn}T_r} \int_0^{T_r} \left[\frac{1}{f_p} \hat{X}_{lmn}^\mp G_{lm} + \left(\frac{2M}{r_p^2 f_p^2} \hat{X}_{lmn}^\mp - \frac{1}{f_p} \frac{d\hat{X}_{lmn}^\mp}{dr} \right) F_{lm} \right] e^{i\omega t} dt, \quad (2.14)$$

where W_{lmn} is the Wronskian

$$W_{lmn} = f \hat{X}_{lmn}^- \frac{d\hat{X}_{lmn}^+}{dr} - f \hat{X}_{lmn}^+ \frac{d\hat{X}_{lmn}^-}{dr}. \quad (2.15)$$

The integral (2.14) is computed using spectral source integration (SSI) [31], in which the integral is replaced by a sum over equally-spaced samples. Because the integrand is periodic in t and smooth, this produces exponential convergence of the result (see [31] and Paper I for more details). This rapid convergence has permitted the MST calculation of the lmn modes of our eccentric-orbit fluxes described in this paper to as many as 450 decimal places of precision.

Once the C_{lmn}^\pm coefficients have been determined, the angular momentum flux at infinity is calculated as

$$\left\langle \frac{dL}{dt} \right\rangle_\infty = \sum_{lmn} \frac{m\omega}{64\pi} \frac{(l+2)!}{(l-2)!} |C_{lmn}^+|^2, \quad (2.16)$$

with the analogous, also standard expression for energy flux at infinity given in Paper I.

III. ANGULAR MOMENTUM RADIATED TO INFINITY: CURRENT COMPLETE PN THEORY AND ADDED ANALYSIS OF HEREDITARY TERMS

Here we review the state of complete PN theory for angular momentum fluxes (known up to 3PN relative order [6, 35]), from which we build new results at higher PN order later in this paper. Additionally, in keeping with a corresponding section in Paper I, we analyze the hereditary (tail) terms of the angular momentum flux expansion, and determine arbitrary-order expansions in eccentricity for those terms. Furthermore, we utilize asymptotic analysis to identify and confirm the singular behavior of enhancement functions as the eccentricity nears unity. Brief summaries of the methods and the quasi-Keplerian representation of the orbital motion are also given in Paper I [21].

A. Instantaneous angular momentum flux terms

Just as in the original articles and Paper I, we use the quasi-Keplerian time eccentricity, e_t , which differs from the Darwin eccentricity, e , described earlier in the paper. Focusing only on the terms that are lowest order in the mass ratio ν (in keeping with present BHPT), the instantaneous contributions to the orbit-averaged angular momentum flux through 3PN can be written as

$$\left\langle \frac{dL}{dt} \right\rangle_\infty^{\text{inst}} = \frac{32}{5} \frac{\mu^2}{M} y^{7/2} (\mathcal{N}_0 + y\mathcal{N}_1 + y^2\mathcal{N}_2 + y^3\mathcal{N}_3), \quad (3.1)$$

where again $y = (M\Omega_\varphi)^{2/3}$ is the compactness parameter, and where

$$\mathcal{N}_0 = \frac{1}{(1 - e_t^2)^2} \left(1 + \frac{7}{8} e_t^2 \right), \quad (3.2)$$

$$\mathcal{N}_1 = \frac{1}{(1 - e_t^2)^3} \left(-\frac{1247}{336} + \frac{3019}{336} e_t^2 + \frac{8399}{2688} e_t^4 \right), \quad (3.3)$$

$$\mathcal{N}_2 = \frac{1}{(1 - e_t^2)^4} \left[-\frac{135431}{9072} - \frac{598435}{6048} e_t^2 + \frac{30271}{3456} e_t^4 + \frac{30505}{16128} e_t^6 + \sqrt{1 - e_t^2} \left(10 + \frac{335}{8} e_t^2 + \frac{35}{8} e_t^4 \right) \right], \quad (3.4)$$

$$\mathcal{N}_3 = \frac{1}{(1 - e_t^2)^5} \left[\frac{2017023341}{9979200} + \frac{270214177}{623700} e_t^2 - \frac{6350078491}{13305600} e_t^4 - \frac{272636461}{4435200} e_t^6 - \frac{10305073}{5677056} e_t^8 \right]$$

$$+ \sqrt{1 - e_t^2} \left(-\frac{379223}{5040} + \frac{309083}{2520} e_t^2 + \frac{13147661}{40320} e_t^4 + \frac{35}{4} e_t^6 \right) \Big] + \frac{1712}{105} \tilde{F}(e_t) \log \left[\frac{y}{y_0} \frac{1 + \sqrt{1 - e_t^2}}{2(1 - e_t^2)} \right], \quad (3.5)$$

are the functions of time eccentricity derived in prior work [35]. Note that y_0 depends on r_0 (a parameter defined in the original paper), which is an arbitrary length scale and which cancels in the total flux. The expressions above are similar to (4.11) of [35], but with a different overall scaling and are expressed in modified harmonic gauge. The function $\tilde{F}(e_t)$ is given by

$$\tilde{F}(e_t) = \frac{1}{(1 - e_t^2)^5} \left(1 + \frac{229}{32} e_t^2 + \frac{327}{64} e_t^4 + \frac{69}{256} e_t^6 \right). \quad (3.6)$$

Any appearance of a tilde over a function name, as in $\tilde{F}(e_t)$, refers to angular momentum, while a corresponding function (in this case $F(e_t)$) without a tilde appears in the energy flux expansion.

B. Hereditary angular momentum flux terms through 3PN order

As with the energy flux (c.f. Paper I), the hereditary portion of the angular momentum flux can be defined in terms of a set of enhancement functions [35–37, 55, 56],

$$\left\langle \frac{dL}{dt} \right\rangle_{\infty}^{\text{hered}} = \frac{32}{5} \frac{\mu^2}{M} y^{7/2} \left\{ 4\pi y^{3/2} \tilde{\varphi}(e_t) - \frac{8191}{672} \pi y^{5/2} \tilde{\psi}(e_t) + y^3 \left(-\frac{1712}{105} \tilde{\chi}(e_t) + \left[-\frac{116761}{3675} + \frac{16}{3} \pi^2 - \frac{1712}{105} \gamma_E - \frac{1712}{105} \log \left(\frac{4y^{3/2}}{y_0} \right) \right] \tilde{F}(e_t) \right) \right\}. \quad (3.7)$$

Here, $\tilde{\varphi}(e_t)$ is the 1.5PN tail term; $\tilde{\psi}(e_t)$ is the 1PN correction to the tail; and the 3PN portion involves $\tilde{\chi}(e_t)$ and $\tilde{F}(e_t)$ and emerges upon combining the angular momentum tail-of-tails and tail² contributions. Unlike the instantaneous terms \mathcal{N}_i , the functions $\tilde{\varphi}(e_t)$, $\tilde{\psi}(e_t)$, and $\tilde{\chi}(e_t)$ admit no simple closed forms. Arun *et al.* originally calculated these contributions numerically but also produced a low-order expansion through e_t^4 for each enhancement function [35].

These expressions are written as functions of the time eccentricity e_t . However, as we will see, the 1.5PN tail $\tilde{\varphi}$ and the functions \tilde{F} and $\tilde{\chi}$ depend only on Newtonian order quantities. Hence, for these functions (as well as \mathcal{N}_0) there is no distinction between using e_t and the usual Keplerian eccentricity. Nevertheless, we will keep the notation consistent by expressing everything here in terms of e_t . Finally, each of these functions is defined to equal 1 in the case of a circular orbit (in keeping with the meaning of an enhancement function) except for $\tilde{\chi}$, which limits to 0 as $e_t \rightarrow 0$.

C. Arbitrary-order expansions for hereditary terms

Previous expressions for the expansions of the tail terms were too limited for our purposes (with the exception of $\tilde{F}(e_t)$ which is exact). We sought arbitrary-order expansions of these terms and applied the methods used in Paper I. The majority of these functions are best handled in the FD. There the Fourier decomposition of the (dimensionless) Newtonian trace-free quadrupole moment [35–37] can be used with the leading-order angular momentum flux to calculate $\mathcal{N}_0(e_t)$

$$\begin{aligned} \mathcal{N}_0(e_t) &= \frac{-i}{16} \epsilon_{ijk} \hat{L}_i \left\langle \ddot{\hat{I}}_{ja}^{(N)} \ddot{\hat{I}}_{ka}^{(N)} \right\rangle \\ &= \frac{-i}{8} \epsilon_{ijk} \hat{L}_i \sum_{n=1}^{\infty} n^5 \hat{f}_{(n)ja}^{(N)} \hat{f}_{(n)ka}^{*(N)} = \sum_{n=1}^{\infty} \tilde{g}(n, e_t) \\ &= \tilde{f}(e_t) = \frac{1}{(1 - e_t^2)^2} \left(1 + \frac{7}{8} e_t^2 \right). \end{aligned} \quad (3.8)$$

Here, $\tilde{f}(e_t)$ is just alternate notation for $\mathcal{N}_0(e_t)$ and is the angular momentum analogue of the traditional Peters-Mathews function $f(e_t)$ (first derived by Peters in [57]) for the quadrupole energy flux. In this expression, ${}_{(n)}\hat{I}_{ij}^{(N)}$ is the n th Fourier harmonic of the dimensionless (Newtonian) quadrupole moment (see Sections III through V of [36]). The product of terms yielding the angular momentum flux radiated into each harmonic is compactly expressed as the function $\tilde{g}(n, e_t)$. This power spectrum for angular momentum flux is given by

$$\begin{aligned} \tilde{g}(n, e_t) &\equiv \sqrt{1 - e_t^2} \left\{ \left(-\frac{2}{e_t^2} + 2 \right) n^2 J'_n(ne_t)^2 \right. \\ &\quad + \left[-\frac{2}{e_t^4} + \frac{3}{e_t^2} - 1 \right] n^2 J_n(ne_t)^2 \\ &\quad + \left[2e_t n^2 + \frac{2}{e_t^3} (1 + n^2) - \frac{1}{e_t} (1 + 4n^2) \right] n \\ &\quad \left. J_n(ne_t) J'_n(ne_t) \right\}. \end{aligned} \quad (3.9)$$

As Arun *et al.* [35] make clear, three of the desired hereditary functions – $\tilde{F}(e_t)$, $\tilde{\varphi}(e_t)$, and $\tilde{\chi}(e_t)$ – follow immediately from knowledge of just this quadrupole spectrum

$$\tilde{F}(e_t) = \frac{1}{4} \sum_{n=1}^{\infty} n^2 \tilde{g}(n, e_t), \quad (3.10)$$

$$\tilde{\varphi}(e_t) = \frac{1}{2} \sum_{n=1}^{\infty} n \tilde{g}(n, e_t), \quad (3.11)$$

$$\tilde{\chi}(e_t) = \frac{1}{4} \sum_{n=1}^{\infty} n^2 \log\left(\frac{n}{2}\right) \tilde{g}(n, e_t). \quad (3.12)$$

Unfortunately, unlike $\tilde{f}(e_t)$ and $\tilde{F}(e_t)$, the latter two sums likely do not admit closed form expressions. This stems from the odd power of n in $\tilde{\varphi}(e_t)$ and the logarithm in $\tilde{\chi}(e_t)$, which give the two sums complicated representations in the time domain and preclude the ability to calculate the time integral over a libration.

As shown in Paper I, however, it is still possible to extract arbitrary-order expansions for sums of these types. Using the Bessel function representation of $\tilde{g}(n, e_t)$ and expanding (3.9) in a Maclaurin series in e_t , we find

$$\begin{aligned} \tilde{g}(n, e_t) = & \left(\frac{n}{2}\right)^{2n-1} e_t^{2n-4} \left(\frac{1}{\Gamma(n-1)^2} \right. \\ & - \frac{n^3 + 3n^2 - 6n + 2}{2\Gamma(n)^2} e_t^2 \\ & \left. + \frac{2n^4 + 15n^3 + 6n^2 - 16n + 2}{16\Gamma(n)^2} e_t^4 + \dots \right). \end{aligned} \quad (3.13)$$

In a sum over n , successive harmonics each contribute a series that starts at a progressively higher power of e_t^2 . Thus, summations like (3.10), (3.11), or (3.12) can be determined to any desired finite order in e_t^2 with only a finite sum (of some length) over n . As in the energy case, the e_t^{-2} and e_t^0 coefficients vanish for $n = 1$, and the $n = 2$ harmonic is the only one that contributes at e_t^0 (and thus for a circular orbit).

Accordingly, we expand the latter two summations from above and find the leading behavior of these functions to be

$$\begin{aligned} \tilde{\varphi}(e_t) = & \frac{1}{(1 - e_t^2)^{7/2}} \left(1 + \frac{97}{32} e_t^2 + \frac{49}{128} e_t^4 - \frac{49}{18432} e_t^6 \right. \\ & - \frac{109}{147456} e_t^8 - \frac{2567}{58982400} e_t^{10} + \frac{4649}{707788800} e_t^{12} \\ & + \frac{418837}{221962567680} e_t^{14} + \frac{28447343}{53271016243200} e_t^{16} \\ & \left. + \frac{5249748289}{19725496300339200} e_t^{18} + \dots \right), \end{aligned} \quad (3.14)$$

$$\begin{aligned} \tilde{\chi}(e_t) = & -\frac{3}{2} \tilde{F}(e_t) \log(1 - e_t^2) + \frac{1}{(1 - e_t^2)^5} \left\{ \right. \\ & \left[-\frac{3}{2} - \frac{549}{32} \log(2) + \frac{2187}{128} \log(3) \right] e_t^2 \\ & \left. + \left[-\frac{735}{64} + \frac{18881}{64} \log(2) - \frac{85293}{512} \log(3) \right] e_t^4 \right\} \end{aligned}$$

$$\begin{aligned} & + \left[-\frac{433}{32} - \frac{6159821}{2304} \log(2) + \frac{5981445}{8192} \log(3) \right. \\ & + \frac{48828125}{73728} \log(5) \left. \right] e_t^6 + \left[-\frac{4193}{512} \right. \\ & + \frac{16811095}{1152} \log(2) + \frac{56772333}{65536} \log(3) \\ & \left. - \frac{4052734375}{589824} \log(5) \right] e_t^8 + \dots \left. \right\}. \end{aligned} \quad (3.15)$$

We give only the first few terms in these power series here. The much lengthier expressions that we have used in our numerical modeling and analytic fitting are given in a MATHEMATICA notebook archived on the Black Hole Perturbation Toolkit website [40]. For computational reference, calculation of over 100 terms in these series in MATHEMATICA requires under 20 seconds on an average laptop. The first four terms of (3.14) are also published in [20].

Both $\tilde{\varphi}$ and $\tilde{\chi}$ diverge as $e_t \rightarrow 1$; however, as displayed in the above equations, both can be written in forms that isolate their divergences. These singular factors will be justified in Section III D, where we analyze the asymptotic behavior near $e_t = 1$ using methods developed in Paper I. Of particular note is the fact that the structure of $\tilde{\chi}$ closely mirrors its energy flux counterpart with a combination of algebraic and logarithmic divergences. We find by direct high-order expansion that the two series have the following limits near $e_t = 1$

$$\tilde{\varphi} \rightarrow \frac{4.41063}{(1 - e_t^2)^{7/2}}, \quad (3.16)$$

$$\tilde{\chi} \rightarrow -\frac{3}{2} \left(\frac{3465}{256} \right) \frac{\log(1 - e_t^2)}{(1 - e_t^2)^5} + \frac{16.7230}{(1 - e_t^2)^5}, \quad (3.17)$$

where $3465/256 \simeq (2/3) 20.3027$ is simply the value of the polynomial portion of $\tilde{F}(e_t)$ evaluated at $e_t = 1$.

As expected from Paper I, the most difficult enhancement function to extract is the 2.5PN term $\tilde{\psi}$. Calculating $\tilde{\psi}$ involves not only the Newtonian mass octupole and current quadrupole moments, but also the 1PN correction to the mass quadrupole moment. At 1PN order the orbital motion no longer closes and corrections to the quadrupole moment require a biperiodic Fourier expansion. Arun *et al.* describe a procedure for computing $\tilde{\psi}$ in [35], which they evaluated numerically. Using a modified form of our expansion methods, we were able to obtain $\tilde{\psi}$ in an expansion out to e_t^{120} , complete with factoring out the relevant eccentricity singular factor. The procedure for using these 1PN multipole moments will be detailed in a future paper [34], where it is shown that not only $\tilde{\psi}$ but an infinite set of 1PN-corrected leading logarithm terms can be derived from the next-most important multipole moments beyond the mass quadrupole. Focusing here just on $\tilde{\psi}(e_t)$, the first few terms in the expansion are

$$\begin{aligned} \tilde{\psi}(e_t) = & \frac{1}{(1 - e_t^2)^{9/2}} \left(1 - \frac{108551}{16382} e_t^2 - \frac{5055125}{524224} e_t^4 - \frac{4125385}{9436032} e_t^6 + \frac{11065099}{603906048} e_t^8 - \frac{68397463}{30195302400} e_t^{10} \right. \\ & - \frac{194038163}{1159499612160} e_t^{12} + \frac{3310841491}{189384936652800} e_t^{14} + \frac{5520081282241}{436342894048051200} e_t^{16} \\ & \left. + \frac{78911659620611}{14137509767156858880} e_t^{18} + \frac{22307748275735593}{8078577009803919360000} e_t^{20} + \dots \right). \end{aligned} \quad (3.18)$$

The power series in the parentheses appears to converge to -15.6906. Again, the more complete expansion is archived at [40].

D. Applying asymptotic analysis to determine eccentricity singular factors

We briefly derive the divergent behavior of the preceding functions as $e_t \rightarrow 1$. The same asymptotic techniques developed in Paper I apply to the angular momentum flux terms. We refer the reader to Paper I for details on the procedure. We note that a comparable analysis of the energy and angular momentum flux asymptotics was undertaken in [58].

Four of the relevant enhancement functions share a dependence on the quadrupole moment spectrum $\tilde{g}(n, e_t)$ found in (3.9) and therefore we require the high eccentricity behavior of this function. To aid our efforts near $e_t = 1$, we define $x \equiv 1 - e_t^2$ and rewrite (3.9) as

$$\begin{aligned} \tilde{g}(n, e_t) = & -n^2 \frac{x^{3/2}(1+x)}{(1-x)^2} J_n(ne_t)^2 - n^2 \frac{2x^{3/2}}{1-x} J'_n(ne_t)^2 \\ & + n \frac{x^{1/2}(1+x+2n^2x^2)}{(1-x)^{3/2}} J_n(ne_t) J'_n(ne_t). \end{aligned} \quad (3.19)$$

From this point on the procedure of Paper I is followed exactly: $J_n(ne_t)$ and $J'_n(ne_t)$ are expressed in terms of their uniform asymptotic expansions for large-order (and large-argument) [59], which have growing importance as $x \rightarrow 0$. This representation involves sums of Airy functions and their derivatives, which must themselves be expanded in the reciprocal of the variable

$$\xi = n \log \left(\frac{1 + \sqrt{x}}{\sqrt{1-x}} \right) - n\sqrt{x} = n\rho(x). \quad (3.20)$$

The various series are inserted into the enhancement function summations, which are then converted from sums over n to integrals over $dn = d\xi/\rho(x)$. Finally, these integrals can be evaluated to extract not only the divergent behavior of the four enhancement functions, but also surprisingly sharp estimates of the numerical limit of the coefficients attached to these divergent terms.

We now apply this asymptotic procedure to the four enhancement functions. The simplest are the two with closed-form expressions. While these terms are already

exactly known, they serve as good tests of the asymptotic analysis. The functions $\tilde{f}(e_t)$ in (3.8) and $\tilde{F}(e_t)$ in (3.10) have known singular dependences of

$$\begin{aligned} \tilde{f}(e_t) & \sim \frac{15}{8} \frac{1}{(1 - e_t^2)^2} = \frac{1.875}{(1 - e_t^2)^2}, \\ \tilde{F}(e_t) & \sim \frac{3465}{256} \frac{1}{(1 - e_t^2)^5} \simeq \frac{13.5352}{(1 - e_t^2)^5}, \end{aligned} \quad (3.21)$$

as $e_t \rightarrow 1$. If we instead make the asymptotic approximations of the sums in (3.8) and (3.10), we find

$$\begin{aligned} \tilde{f}(e_t) & \sim \frac{1141}{192\pi} \frac{1}{(1 - e_t^2)^2} \simeq \frac{1.8916}{(1 - e_t^2)^2}, \\ \tilde{F}(e_t) & \sim \frac{56429761}{1327104\pi} \frac{1}{(1 - e_t^2)^5} \simeq \frac{13.5348}{(1 - e_t^2)^5}, \end{aligned} \quad (3.22)$$

which extracts the correct eccentricity singular functions and yields close estimates of the exact coefficients.

Next we move to $\tilde{\varphi}(e_t)$ and $\tilde{\chi}(e_t)$, which are not known analytically. For $\tilde{\varphi}(e_t)$, the sum in (3.11) leads to the following asymptotic estimate

$$\begin{aligned} \tilde{\varphi}(e_t) & \sim \frac{191287}{13824\pi} \frac{1}{(1 - e_t^2)^{7/2}} - \frac{386929}{34560\pi} \frac{1}{(1 - e_t^2)^{5/2}} + \dots \\ & \simeq \frac{4.40455}{(1 - e_t^2)^{7/2}} - \frac{3.56375}{(1 - e_t^2)^{5/2}} + \dots, \end{aligned} \quad (3.23)$$

where in this case we retained the first and second terms in the expansion about $e_t = 1$. The leading singular factor matches that chosen in (3.14) and its coefficient approximates the 4.41063 value found in (3.16).

The last function of this kind is $\tilde{\chi}(e_t)$, whose definition involves $\log(n/2)$. Using the same asymptotic expansions and integral approximation for the sum, and retaining the first two divergent terms, we find

$$\begin{aligned} \tilde{\chi}(e_t) & \sim -\frac{56429761}{884736\pi} \left[\log(1 - e_t^2) - \frac{79015440}{56429761} \right. \\ & \left. + \frac{2}{3}\gamma_E + \frac{4}{3}\log(2) - \frac{2}{3}\log(3) \right] \frac{1}{(1 - e_t^2)^5} \\ & \approx -20.3023 \frac{\log(1 - e_t^2)}{(1 - e_t^2)^5} + \frac{16.7219}{(1 - e_t^2)^5}. \end{aligned} \quad (3.24)$$

Thus, we see that the form of (3.15), though already verified through direct high-order expansion, is validated by the asymptotic analysis.

The asymptotic analysis confirmed what we already guessed about the closed form for the leading singular term (involving $\tilde{F}(e_t)$) in (3.15) for $\tilde{\chi}(e_t)$, since it resembles strongly its energy counterpart (Paper I). In fact, if we consider making a PN expansion in the orbital parameter $1/p$ instead of y , that specific term in (3.15) with its logarithmic and algebraic divergences is necessary to cancel other logarithmically divergent terms in the full 3PN flux. As a last check, note that the two numerical coefficients in (3.24) compare well with their counterparts in (3.15), which were found to be approximately -20.3027

and $+16.7230$, respectively.

IV. FINDING NEW COEFFICIENTS IN THE FLUXES VIA MODE-BY-MODE FITTING

A. PN expansion from the BHPT viewpoint

We move now beyond known results to calculate new coefficients at higher order in the PN expansion using perturbation theory. To that end, we use the following general form for the angular momentum flux at infinity

$$\begin{aligned} \left\langle \frac{dL}{dt} \right\rangle^\infty &= \left\langle \frac{dL}{dt} \right\rangle_N^\infty \left[\mathcal{J}_0 + y\mathcal{J}_1 + y^{3/2}\mathcal{J}_{3/2} + y^2\mathcal{J}_2 + y^{5/2}\mathcal{J}_{5/2} + y^3 \left(\mathcal{J}_3 + \mathcal{J}_{3L} \log(y) \right) + y^{7/2}\mathcal{J}_{7/2} \right. \\ &+ y^4 \left(\mathcal{J}_4 + \mathcal{J}_{4L} \log(y) \right) + y^{9/2} \left(\mathcal{J}_{9/2} + \mathcal{J}_{9/2L} \log(y) \right) + y^5 \left(\mathcal{J}_5 + \mathcal{J}_{5L} \log(y) \right) \\ &+ y^{11/2} \left(\mathcal{J}_{11/2} + \mathcal{J}_{11/2L} \log(y) \right) + y^6 \left(\mathcal{J}_6 + \mathcal{J}_{6L} \log(y) + \mathcal{J}_{6L^2} \log^2(y) \right) + y^{13/2} \left(\mathcal{J}_{13/2} + \mathcal{J}_{13/2L} \log(y) \right) \\ &+ y^7 \left(\mathcal{J}_7 + \mathcal{J}_{7L} \log(y) + \mathcal{J}_{7L^2} \log^2(y) \right) + y^{15/2} \left(\mathcal{J}_{15/2} + \mathcal{J}_{15/2L} \log(y) + \mathcal{J}_{15/2L^2} \log^2(y) \right) \\ &\left. + y^8 \left(\mathcal{J}_8 + \mathcal{J}_{8L} \log(y) + \mathcal{J}_{8L^2} \log^2(y) \right) + y^{17/2} \left(\mathcal{J}_{17/2} + \mathcal{J}_{17/2L} \log(y) + \mathcal{J}_{17/2L^2} \log^2(y) \right) + \dots \right], \quad (4.1) \end{aligned}$$

where the Newtonian prefactor, as before, is given by

$$\left\langle \frac{dL}{dt} \right\rangle_N^\infty = \frac{32}{5} \frac{\mu^2}{M} y^{7/2}. \quad (4.2)$$

In the above expansion, each $\mathcal{J}_i = \mathcal{J}_i(e)$ represents an eccentricity flux function for the total flux radiated at a PN term scripted by i . Terms in the PN expansion have the form $y^n \log^k(y)$ and the script i encodes both the integer or half-integer for power n of y and the integer power k of $\log(y)$.

There are two changes in this notation over that of Sec. III. First, we transition from using time eccentricity e_t to using Darwin eccentricity e , which is the natural choice for BHPT calculations (see Sec. II A). We have recently derived the relationship between e_t and e to all PN orders [34] at lowest order in the mass ratio. Using that relationship, it is possible to check the results of BHPT fitting against the enhancement functions of Section III through 3PN, thus confirming prior work. Second, in (4.1) we no longer attempt to separate instantaneous and hereditary contributions to the flux functions, since that distinction is not possible with perturbative methods alone. Therefore, we generically use the \mathcal{J}_i notation at all orders to denote the combination.

B. The original fitting scheme

When the orbit is wide (i.e., in the PN regime), the representation (4.1) is a valid expansion for the values that would emerge from evaluating the BHPT flux formula (2.16). We can use (2.16) to derive the analytic form of the functions in (4.1). One way to do this is to directly expand the MST solutions analytically and carry the results through to obtain $|C_{lmn}^\pm|^2$ as a PN expansion (see e.g., [13, 22, 60–64]). However, Paper I used a different approach, evaluating the fluxes numerically and then determining the analytic coefficients. In this approach, the full flux is calculated to some preset accuracy goal for a large number of orbits that vary in p and e . This creates a two-dimensional array of orbital flux values, which can then be fit to the form of the PN expansion in y and e . If the fit is performed with enough accuracy, analytic forms for the coefficients in the \mathcal{J}_i can be extracted from the highly precise numerical results using an integer-relation algorithm [32]. Using this procedure, Paper I showed some of the analytic dependence of the energy flux up to 7PN order, by computing roughly 1700 orbits of varying separation and eccentricity, with roughly ~ 7500 lmn flux components for each orbit and with an overall accuracy of 200 decimal places for the flux relative to the quadrupole mode. We refer the reader to Paper I for details.

It is noteworthy that the two methods (all-analytic and numeric-analytic) are somewhat complementary in nature. We recently began supplementing our fitting results using a new code based on the purely analytic approach. In the process we discovered that while analytic methods are significantly more efficient at reaching high PN order, they have more difficulty attaining high orders in the power series in eccentricity. On the other hand, while the fitting approach becomes unwieldy around 8PN to 12PN order, with enough sampling it can successfully extract nearly arbitrary orders in e^2 —at least when the eccentricity power series coefficients are simple (e.g., all rational numbers). However, when the coefficients instead contain complicated combinations of transcendental numbers, like π^2 and $\log(2)$, the integer-relation algorithm struggles to identify the analytic representation of the decimal number input, unless much higher numerical precision is utilized. More complicated combinations of transcendental numbers are exactly what occurs in certain higher order (integer) PN terms, like $\mathcal{L}_5(e)$ and $\mathcal{L}_6(e)$. As a result, very few coefficients in the power series in eccentricity were extracted in terms like these in Paper I.

Developments in the purely analytic approach will be described in future work [65]. In this paper we show instead a new technique for obtaining a marked improvement in the numerical fitting scheme. It turns out possible to separate key dependences in the eccentricity flux functions and to determine coefficients in a hierarchical fashion. With this modification to the procedure of Paper I we have significantly expanded the understanding of high PN order fluxes. One key to the procedure is to avoid computing and summing all of the lmn modes and then performing one single fit. Instead, we perform the entire fitting process on each lmn mode individually, extracting as many analytic coefficients as we can, and then sum all the results into the final PN expansion. This process has two key advantages over the previous one: it turns out possible in a predictable way to reduce the number of modes that necessarily must be computed and at the individual lmn mode level we find the existence of regular structure in the appearance of transcendental coefficients, which can be exploited in the fitting process.

C. Reducing the number of flux calculations

As noted above, calculations of the full energy flux for each orbit, characterized by a unique combination of p and e , required around 7500 lmn modes, each of which had to be computed to an accuracy sufficient to make the net flux accurate to 200 decimal places. With over 1700 combinations of p and e needed for the fit, the total number of modes computed numbered over ten million. However, by fitting each lmn separately, this number can be reduced significantly. This works as follows. We set first a particular goal in power of eccentricity to be reached. We chose e^{30} for our purposes. This power of eccentricity

becomes a hard limit, sacrificing any ability to find analytic coefficients beyond it. Yet a benefit results, because each lmn mode can be written as a power series in eccentricity starting with $e^{2|n|}$, and so no modes with $|n|$ beyond 15 need be calculated, which leaves us with just 31 n modes for each spherical harmonic lm .

By counting the lm modes that would be needed to reach 7PN (the goal in Paper I), we find that this would reduce the necessary mode calculations to about 1450 for each orbit (p, e), a five-fold reduction. Additional gain might be made by setting the eccentricity expansion goals to vary by PN order, thus potentially lowering this number further.

D. Transcendental structure and the eulerlog function

As Paper I showed, in the PN expansion the most significant bottleneck in the extraction of analytic coefficients is the appearance of transcendental numbers at higher orders. These begin at 3PN order and increase in complexity each 3PN thereafter. For instance, the circular-orbit limit of the angular momentum flux at 4PN order is given by

$$\mathcal{J}_4^{\text{circ}} = -\frac{323105549467}{3178375200} + \frac{232597}{4410}\gamma_E - \frac{1369}{126}\pi^2 + \frac{39931}{294}\log(2) - \frac{47385}{1568}\log(3). \quad (4.3)$$

In general, as is clear from the 3PN hereditary function $\tilde{\chi}(e)$ and from recent work [34] at 4PN order, the 3PN, 4PN, and 5PN non-log terms will (without isolating any eccentricity singular factors) have the form

$$\mathcal{J}_q = \sum_{i=1}^{\infty} e^{2i} \left(a_i + b_i \pi^2 + c_i \gamma_E + d_i \log 2 + e_i \log 3 + f_i \log 5 + g_i \log 7 + \dots \right), \quad (4.4)$$

where $q \in \{3, 4, 5\}$ and the coefficients in the sets (a_i, b_i, c_i, \dots) are all rational numbers that vary with q . Note that the natural log of each prime will first appear at some sufficiently high i and then will remain present at every PN order thereafter. Because for a given i each coefficient (a_i, b_i, c_i, \dots) is different, all of these coefficients must be found simultaneously by an integer-relation algorithm using a multi-dimensional search vector, e.g., $\{1, \pi^2, \gamma_E, \log(2), \log(3)\}$ (the dimension of the search vector is set by the number of unique transcendental numbers plus one for the rationals themselves; i.e., five dimensional in the example given). This drastically reduces the ability of the integer-relation algorithm to find analytic coefficients, unless numerical precision is raised significantly.

Fitting by lmn (or even just lm) modes aids this effort because of how the transcendental structure of individual modes differs from that of the full flux. To elaborate, it

is well known that only the $l = 2, m = 2$ and $l = 2, m = -2$ modes contribute to the Peters flux \mathcal{J}_0 . The PN expansions of all other lm modes begin at higher powers of y . Specifically, any given mode will be suppressed by a factor of y^r [33], where

$$r = \begin{cases} l - 2 & l + m \text{ even,} \\ l - 1 & l + m \text{ odd.} \end{cases} \quad (4.5)$$

This being the case, the PN expansion of an individual lm mode will have a form that differs from (4.1) and is found to be instead

$$\begin{aligned} \left\langle \frac{dL}{dt} \right\rangle_{lm}^\infty &= \sum_n \frac{m\omega}{64\pi} \frac{(l+2)!}{(l-2)!} |C_{lmn}^+|^2 \\ &= \left\langle \frac{dL}{dt} \right\rangle_N^\infty y^r \left[\mathcal{J}_0^{lm} + y \mathcal{J}_1^{lm} + y^{3/2} \mathcal{J}_{3/2}^{lm} + y^2 \mathcal{J}_2^{lm} \right. \\ &\quad \left. + y^{5/2} \mathcal{J}_{5/2}^{lm} + y^3 \left(\mathcal{J}_3^{lm} + \mathcal{J}_{3L}^{lm} \log(y) \right) + \dots \right]. \end{aligned} \quad (4.6)$$

(Note that there is a slight subtlety in this notation, as \mathcal{J}_i^{lm} does not represent a decomposition of \mathcal{J}_i , but rather the i th *relative-order* flux term in the lm mode.) We can immediately see from this expansion that the lowest appearance of transcendental numbers will be in \mathcal{J}_3^{lm} , which contributes to the term \mathcal{J}_{r+3} in the full flux. As an example, consider the $l = 4, m = 3$ mode, for which $r = 3$. This mode will not contain a term with the eccentric transcendental structure (4.4) until 6PN relative to \mathcal{J}_0 . Therefore, in calculating full flux coefficients at, say, 4PN order, this mode will only contribute rational numbers, which require less numerical precision to extract.

The PN series for an lmn mode will mirror (4.6), but with $lm \rightarrow lmn$ (the exception to this is when $m = -n$; see Sec. IV F). Therefore, in fitting by lmn , rather than place a universal precision goal to be met across the board, we vary the number of significant decimal places to which we calculate in a planned fashion by mode to account for this changing transcendental structure. This improvement is a useful but fairly modest one, as the precision needs for even a small number of lmn modes quickly become prohibitively expensive once the search vector surpasses five terms.

Fortunately, there is another key difference between the transcendental structure of the full flux and that of its lmn modes—the appearance of the eulerlog function. It is well known and studied [33] that for the lm modes of a circular-orbit flux, at 3/4/5PN (integer) orders the sum of the non-log and log terms has the form

$$\begin{aligned} \mathcal{J}_q^{lm, \text{circ}} + \mathcal{J}_{qL}^{lm, \text{circ}} \log y &= a_0 + b_0 \pi^2 \\ &+ c_0 \left(\gamma_E + \log 2 + \log |m| + \frac{1}{2} \log y \right) \quad (m \neq 0), \end{aligned} \quad (4.7)$$

where the rational coefficients $\{a_0, b_0, c_0\}$ vary with both q and lm . Because the same coefficient sits in front of all of the transcendentals $\gamma_E, \log 2, \log |m|$, and the factor

$(1/2) \log y$ [33, 38], these factors are all grouped together into defining the eulerlog function:

$$\text{eulerlog}_m(y) = \gamma_E + \log 2 + \log |m| + \frac{1}{2} \log y. \quad (4.8)$$

Thus, in these circular-orbit cases, the number of independent rational coefficients reduces to three. This convenient reduction is lost when the modes are summed over m , as the log terms will accumulate coefficients that can no longer be related to one another.

As it turns out, the lmn modes of the flux for eccentric orbits admit an analog of this eulerlog function. When separated by lmn mode, (4.4) and (4.7) generalize to

$$\begin{aligned} \mathcal{J}_q^{lmn} + \mathcal{J}_{qL}^{lmn} \log y &= \sum_{i=|n|}^{\infty} e^{2i} \left[a_i + b_i \pi^2 \right. \\ &\quad \left. + c_i \left(\gamma_E + \log 2 + \log |m + n| + \frac{1}{2} \log y \right) \right], \end{aligned} \quad (4.9)$$

for $m \neq -n$. This allowed us to define a generalized eulerlog function (for $m \neq -n$) that is given by

$$\text{eulerlog}_{m,n}(y) = \gamma_E + \log 2 + \log |m + n| + \frac{1}{2} \log y. \quad (4.10)$$

We discovered this function while working with lmn mode fitting, but Nathan Johnson-McDaniel in 2015 was actually the first to find the generalized eulerlog function $\text{eulerlog}_{m,n}(y)$ by modifying his S_{lm} factorization [33]. By using this function while fitting, the search vector required for the integer-relation algorithm immediately drops from five or more terms down to three.

E. Hierarchical fitting: the eulerlog simplification

Because the generalized eulerlog function includes the $\log(y)$ term, we can improve the fitting process even further. Taking any of the 3/4/5PN series again and using the expected general form (4.9) as our model, we note that the $\log(y)$ term (\mathcal{J}_{qL}^{lmn}) is simply a rational power series in e^2 — one which can be fit separately from the more complicated non-log term (\mathcal{J}_q^{lmn}). By fitting this log series first we can determine the c_i coefficients independently. Once these coefficients are known, we can return attention to the more complicated non-log flux term. Then, applying knowledge of the eulerlog function, we see that the c_i coefficients are also the ones that stand on the combination of transcendentals, $\gamma_E + \log 2 + \log |m + n|$. With this piece subtracted off, we are left with a remaining search vector with only two terms, $\{1, \pi^2\}$.

Better still, Johnson-McDaniel's progress on tail factorizations (both circular in [33] and more recently eccentric) suggests that the π^2 piece is also linked to this eulerlog function. We have in fact discovered empirically that the ratio of b_i to c_i in (4.9) depends exclusively on l , allowing a generalization of the eulerlog function to what

might be called the ‘‘eulerlogpi’’ function. This connection was used as a further aid in extracting a few more coefficients in some of the high PN terms (shown in Secs. V and VI), but we leave discussion of structure beyond the eulerlog function to a later paper.

Up to this point we have only discussed simplifications to terms at PN orders 3, 4, and 5. However, the eulerlog function at least partially characterizes the appearance of those particular transcendentals, and their products, at even higher orders. Specifically, for each integer $k \geq 1$, \mathcal{J}_{3k}^{lmn} , \mathcal{J}_{3k+1}^{lmn} , and \mathcal{J}_{3k+2}^{lmn} will all contain a product of k terms, each having the form of the square-bracketed portion in (4.9), though there may also be additional transcendentals native to that order (such as $\zeta(3)$). An analog of this fact was also applied in [17] to simplify the lm modes of the redshift invariant in the circular-orbit limit.

As an example, consider the sum of the 6PN non-log, log, and log-squared enhancement functions. This sum can be shown to decompose into

$$\begin{aligned} & \mathcal{J}_6^{lmn} + \mathcal{J}_{6L}^{lmn} \log y + \mathcal{J}_{6L^2}^{lmn} (\log y)^2 \\ &= \sum_{i=|n|}^{\infty} e^{2i} \left[a_i + b_i \pi^2 + c_i \pi^4 + d_i \zeta(3) \right. \\ &+ \left(e_i + f_i \pi^2 + g_i \text{eulerlog}_{m,n}(y) \right) \\ &\left. \times \left(h_i + j_i \pi^2 + k_i \text{eulerlog}_{m,n}(y) \right) \right]. \quad (4.11) \end{aligned}$$

We can see the aforementioned product involving the eulerlog function, and also the first appearance of the new transcendental, $\zeta(3)$. As it turns out, this expression is more complicated than it has to be and contains more than the true number of degrees of freedom. With a bit of inspection, we can write (4.11) in the simpler form

$$\begin{aligned} & \mathcal{J}_6^{lmn} + \mathcal{J}_{6L}^{lmn} \log y + \mathcal{J}_{6L^2}^{lmn} (\log y)^2 \\ &= \sum_{i=|n|}^{\infty} e^{2i} \left[a_i + b_i \pi^2 + c_i \pi^4 + d_i \zeta(3) \right. \\ &+ \left(e_i + f_i \pi^2 + g_i \text{eulerlog}_{m,n}(y) \right) \\ &\left. \times \left(1 + h_i \pi^2 + \text{eulerlog}_{m,n}(y) \right) \right]. \quad (4.12) \end{aligned}$$

After multiplying out the summands, collecting terms, and renaming coefficients, we can separate the terms with different powers of $\log(y)$ to obtain

$$\mathcal{J}_{6L^2}^{lmn} = \sum_{i=|n|}^{\infty} e^{2i} \left(\frac{C_i}{4} \right), \quad (4.13)$$

$$\mathcal{J}_{6L}^{lmn} = \sum_{i=|n|}^{\infty} e^{2i} \left(A_i + B_i \pi^2 + C_i \beta \right), \quad (4.14)$$

$$\mathcal{J}_6^{lmn} = \sum_{i=|n|}^{\infty} e^{2i} \left(2A_i \beta + 2B_i \pi^2 \beta + C_i \beta^2 \right)$$

$$+ D_i + E_i \pi^2 + F_i \pi^4 + G_i \zeta(3). \quad (4.15)$$

Here we define $\beta = \gamma_E + \log 2 + \log |m+n|$. Remarkably, by working from the top down and carrying over results, we can ascertain the full analytic structure at 6PN, including the hardest non-log term, of each lmn mode with a search vector of maximum length of four. Without this hierarchical procedure the required search vector would be $\{1, \pi^2, \gamma_E, \log 2, \log |m+n| \pi^2 \gamma_E, \pi^2 \log 2, \pi \log |m+n|, \gamma_E \log 2, \gamma_E \log |m+n|, \log 2 \log |m+n|, \pi^4, \gamma_E^2, (\log 2)^2, (\log |m+n|)^2, \zeta(3)\}$ (i.e., 15 dimensional!), which would likely preclude ever finding the analytic fit by direct application of the integer-relation algorithm.

Though this hierarchical fitting method also works perfectly as just described for 7PN, it (perhaps unexpectedly) requires modification at 8PN order. As can be seen in the circular-orbit results of [33], 8PN marks the first appearance of the $\log(2y)$ contribution, separate from the eulerlog function. While the $\log(2y)$ term can be separated, it alters the balance between the $\log(y)$ and $\log(2)$ factors and alters the transition from (4.9) to (4.11). The situation at 8PN can be salvaged by introducing a 5th search vector component of $2\beta - \log(2)$, though doing so significantly decreases the ability to find complete analytic fits without increasing numerical precision.

F. Modes with $m = -n$

Omitted from the above analysis is what to do with all modes for which $m = -n$. In these cases the eulerlog function, as previously defined in (4.10), is divergent and not useful. The reason these flux components represent a special case is that the frequency $\omega = m\Omega_\varphi + n\Omega_r$ of each of these $m = -n$ modes almost vanishes and appears at one PN order higher than neighboring modes, because $\Omega_\varphi \rightarrow \Omega_r$ in the Newtonian limit. As a result, the lowest power of y appearing in each of these modes is $2l+1$ higher ($2l+2$ for the energy flux) than it would be otherwise (thus yielding total order $3l-1$ for $l+m$ even and $3l$ for $l+m$ odd relative to \mathcal{J}_0). Hence, there are no contributions until 5PN order. Unlike cases where $m \neq -n$, these modes produce no contribution at 1.5PN and so no combinations of transcendentals appear until 5PN order. When transcendentals do appear, they are characterized by a different eulerlog function of the form

$$\text{eulerlog}_{m,-m}(y) = \gamma_E + \log 6 + \log m + \frac{3}{2} \log y. \quad (4.16)$$

Thus, if we restrict attention to the $m = -n$ contributions, the structure of the sum of the non-log and log terms that contribute at the 5/6/7PN level relative to the lowest order for that l is

$$\mathcal{J}_{5/6/7}^{lm-m} + \mathcal{J}_{5L/6L/7L}^{lm-m} \log y = \sum_{i=|n|}^{\infty} e^{2i} \left[a_i + b_i \pi^2 \right]$$

$$+ c_i \left(\gamma_E + \log 6 + \log m + \frac{3}{2} \log y \right) \Big]. \quad (4.17)$$

The net effect is that the first appearance of such a series will be at 10PN relative to \mathcal{J}_0 .

To round out this discussion, note that no $m = 0$ modes contribute to the angular momentum flux (see (2.16)), while only those modes with $m = n = 0$ vanish in the energy flux case. Finally, in both fluxes lmn modes are equal to $l,-m,-n$ modes.

G. Validation

Irrespective of finding substantial improvements in fitting, the same issue is still faced here as it was in Paper I—how do we know that the analytic results emerging from an “experimental mathematics” technique are not simply a coincidence? After all, it is always possible to represent a floating point number of any precision as a rational number or as a transcendental times a rational number. An integer-relation algorithm can potentially return multiple solutions for the same numeric input. We need some means of testing to be confident that a retrieved rational number, or sum of rationals times transcendentals, is in fact the correct one which would emerge from a first-principles analytic calculation. Fortunately, several validation tests exist.

The simplest, as noted in Paper I, can be applied to any derived rational coefficient. For any rational number in irreducible form with the coprime integers having N_N digits in the numerator and N_D digits in the denominator, define the *fractional complexity* f by $f = N_D + N_N$. Say it is suspected that a rational with complexity f represents a given decimal number, and that the decimal number and rational agree to N digits of precision. Then, the probability that the rational number lies within the uncertainty range of the decimal number but is a mere coincidence is roughly given by $\mathcal{P} \simeq 10^{f-N}$ [14]. Using this test alone, many of the coefficients that we obtain, for the subset of PN series that only have rational coefficients, have *extremely* small chances of coincidence—as low as 10^{-300} in some cases. Moving one step further, at certain PN orders involving the eulerlog simplification, like 9/2PN and 11/2PN, we can use this formula successfully to confirm that the procedure is not producing results that are mere coincidence. To be more specific, with the hierarchical procedure we first check that the log series, with its expected rational coefficients, has essentially zero chance of coincidence. Then we apply the step of removing the eulerlog term with its transcendentals from the non-log flux and use the integer-relational algorithm to determine remaining rational coefficients. These are then subjected to the same test, with the requirement that they too have near vanishing chance of coincidence. If the extraction fails, the fractional complexity of the derived rationals will be large and the probabilities of coincidence will jump many orders of magnitude. This

is the usual indication we get when we reach the limit of being able to determine a high PN order fit.

For series that are not purely rational (e.g., 6PN) and one of the integer-relation fits is being made in multiple dimensions, verification requires a slightly subtler technique, as the above expression cannot account for the greater dimension of the search vector space. One possible extension would be to add up all the digits of all the coprimes in the rational numbers to use as a substitute formula for \mathcal{P} . However, such a probability test is not as well validated as its single rational counterpart.

A useful second test, available for all emergent rational numbers, is to examine the prime factorization of each term’s overall denominator, as these factorizations exhibit a certain universal behavior. In any given power series in eccentricity, this behavior involves the largest prime p_i that appears in the common denominator of the coefficient of the e^{2i} term. An analytic inspection of the RWZ formalism reveals that this prime should remain within an order of magnitude of the limit $p_i \sim i$, though with somewhat larger p_i occurring at higher PN order. Every single rational number denominator that we have encountered through 9PN has $p_i \leq 29$. In number theory, large integers whose prime factorization only involves small primes, or powers of small primes, up to p_i are called p_i -smooth numbers. Furthermore, number theory considerations show [66] that the probability that a randomly selected denominator with d digits will have all prime factors $\leq p_i$ is less than

$$\frac{1}{10^{d+1} - 10^d} \left(\frac{[(d+1) \log(10)/\log(2)] + \pi(p_i)}{\pi(p_i)} \right), \quad (4.18)$$

where $\binom{a}{b}$ is the binomial coefficient and $\pi(p_i)$ is the prime counting function (the number of primes $\leq p_i$). This condition has been utilized also in [17]. As an example, in the 202 mode, the coefficient of e^6 at 6PN order has a denominator equal to 1150293142462464000. For this number, $d = 20$ and the maximum prime is $p_3 = 17$. Therefore, the probability of an integer of this size being 17-smooth is of order 10^{-11} . Another quick check, as reflected in this example, is that denominators for high powers of e^2 and y will be characterized by powers of 10 (though this does not apply for modes where 5 divides $|m+n|$).

Finally, we have identified a fairly intuitive universal trend characterizing the PN series of lmn modes, which involves the fractional complexity directly. Consider a given PN order and the power series in eccentricity at that order. It can be easily seen that the fractional complexity of the rational numbers in the eccentricity series generally increases with powers of e (i.e., the rational numbers get more “complicated” for higher powers of e^2). But as we vary the PN order the precise values of f at the same power of e differ greatly, both because of a different power of y and because transcendentals may or may not be attached to the particular rational number. We can see both aspects of this behavior on the left side of Fig. 1. There we plot f versus the exponent

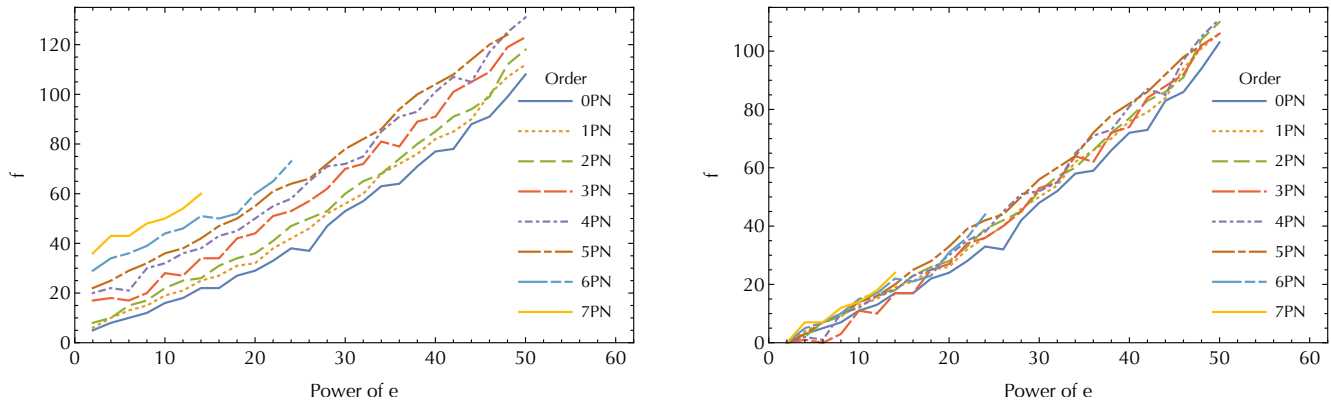


FIG. 1. Increase of the fractional complexity f with eccentricity power series exponent, separated by PN order. For orders 3PN and above, the purely rational coefficient is used. On the left, we plot data from the $lmn = (2, 2, 1)$ mode for multiple PN orders. On the right, each trend has been normalized by subtracting the first value of f in the sequence, leading to a more universal growth in complexity.

of eccentricity e extracted from a set of different series. The first behavior is clearly evident as all of the curves have roughly the same shape. However, it is also clear that the curves differ significantly as each has effectively an offset corresponding to PN order. We then normalize these trends by taking each sequence and subtracting off the first value of f in each sequence. The results are plotted on the right side, which illustrates a more universal behavior. This universal trend in fractional complexity serves as a third test for the integer-relation algorithm results. We compare the f values of rational numbers extracted in a series to this trend, looking for any values that represent clear outliers.

H. The roadmap for fitting by lmn modes

Here we present the full procedural roadmap for extracting eccentricity coefficients in the high PN order series from BHPT flux calculations. An analogous roadmap was given in Paper I, with much more detail on the BHPT steps, and should be consulted as well.

- *Solve orbit equations for given p and e .* Given a set of orbital parameters, we find $t_p(\chi)$, $\varphi_p(\chi)$, and $r_p(\chi)$ to high accuracy at locations equally spaced in χ using SSI. From these functions we also obtain the orbital frequencies Ω_r and Ω_φ .
- *Obtain homogeneous solutions to the FD RWZ master equation for given lmn mode.* We find the (normalized) homogeneous solutions to (2.10) using the MST formalism and transformations outlined in Paper I. All quantities are computed with some pre-determined, mode-dependent accuracy goal; in this paper that goal ranged from 450 decimals for the 20 and 22 modes to 150 decimals for $l = 8$ and above.

- *Form lmn flux contribution.* Form C_{lmn}^+ by applying the exponentially-convergent SSI technique to (2.14). The coefficient C_{lmn}^+ feeds into a single positive-definite term in the sum (2.16). Unlike in Paper I, here we leave the flux data in this lmn component form.

The next steps involve the PN-side computations:

- *Select fitting goals for y and e .* We set a hard limit of 8.5PN order in y and 30th order in e . Thus, we compute lmn fluxes for $l \leq 10$, $0 \leq m \leq l$ (and only even m for $l = 10$), and $-15 \leq n \leq 15$. Because the fitting is done separately for each mode, we are not restricted to any universal choices of p and e , and we can wildly vary our accuracy goals with l, m , and n . For optimal results, we increased the number of p and e values for low l and m , computing as many as 2750 orbits for the 220 mode and as few as 1300 orbits for all $l = 10$ modes. In general, e values ranged from 10^{-5} to 0.1, while p values ranged anywhere from 10^8 through 10^{55} , depending on mode. The values of y are derived from p and e .
- *Use expected form of the expansion in y .* Known results for circular fluxes on Schwarzschild backgrounds allow us to surmise the expected terms in the y -expansion, shown in Eqn. (4.1). In mode-by-mode fitting this form is adjusted by an overall factor of y^r , where $r = l - 2$ if $l + m$ is even and $r = l - 1$ if $l + m$ is odd.
- *Fit for terms on powers of y and $\log(y)$.* We use MATHEMATICA's `NonlinearModelFit` function to obtain numerical values for the coefficients $\mathcal{J}_{7/2}^{lmn}$, \mathcal{J}_4^{lmn} , etc. We perform this fit separately for each of the values of e in a mode's dataset.
- *Fit each model for chosen $\mathcal{J}_i^{lmn}(e)$ using eccentricity-dependent data, starting with the highest power of \log .* The function `NonlinearModelFit` is again used to find

the unknown coefficients in each eccentricity function expansion. The eccentricity coefficient models allow us to perform hierarchical fitting. As lower order e coefficients are firmly determined in analytic form (see next step), they can be eliminated in the fitting model to allow new, higher-order ones to be included. In keeping with the eulerlog procedure, we first fit the highest $\log(y)$ power appearing at any given order.

- *Attempt to determine analytic form of e^2 coefficients.* Because we have chosen the highest power of \log at this order, the fitted series will necessarily be rational. We use MATHEMATICA's function `RootApproximant` (hereafter RA), which finds simple fractional representations for rational coefficients only. As we progress to more complicated terms, transcendentals will begin to appear, and we will require MATHEMATICA's `FindIntegerNullVector` (hereafter FINV), which is an implementation of the PSLQ integer-relation algorithm.
- *Assess the validity of the analytic coefficients.* A rational or irrational number, or combination thereof, predicted by RA or FINV to represent a given decimal number has a certain probability of being a coincidence (Note: the output will be a very accurate *representation* of the input decimal number regardless). The specifics of this determination, as well as various additional consistency checks, are given in Section IV G. With the analytic coefficients we obtain, in no case is the probability of coincidence larger than 10^{-6} , and in many cases the probability is as low as 10^{-300} . It is also important that the analytic output of PSLQ not change when the number of significant digits in the input is varied (within some range).
- *If necessary, move sequentially down in powers of \log at the same order, fitting each new term via the corresponding eulerlog simplification.* Once the rational series is taken to the limits of precision for a given $\log(y)^k$, it can be multiplied by the appropriate eulerlog factors and subtracted off the fit data for the $\log(y)^{k-1}$ term. As shown in previous sections, this new series will be more complicated than that for $\log(y)^k$, but it will typically still be tractable. In this way, we fit all log powers (including the non-log terms with power 0) for a single PN order (power of y) together. We perform this fit for all unknown PN orders through 8.5PN. We are also able to retrieve the term \mathcal{J}_{9L3} , which admits a closed form expression.
- *Sum over lmn modes.* We repeat the steps above for each lmn component of the flux. Then, we reconstruct

the total flux at each PN order by summing: first over $-15 \leq n \leq 15$, then over $0 \leq m \leq l$, and then over $2 \leq l \leq 10$. Finally, with the full flux summed at a given PN order, a predicted eccentricity singular factor is divided out of the expression, often leaving a convergent power series. Note that this procedure allows us to save our data by both lm and lmn modes. Segregating results by lm modes can allow the use of known or expected PN forms to turn some truncated infinite series into exact, closed-form or simplified expressions with appropriate eccentricity singular factors.

V. ANGULAR MOMENTUM RADIATION: NEW COEFFICIENTS THROUGH 8.5PN ORDER

A. Results

We now provide the understanding we have gained of the high-order terms in the PN expansions of the angular momentum flux (at lowest order in the mass ratio ν). The expansion is given sequentially to 8.5PN order relative to the leading (Newtonian) term. We attempted to take all eccentricity power series to e^{30} analytically, but we substituted numeric forms when necessary. As a result, we have accurate mixed analytic/numeric results to e^{30} for all PN orders except the 8PN non-log term, which was only completed to e^{10} . In some cases, we have additional numeric results beyond e^{30} from the full-flux fitting method of Paper I. We also give the 9PN $(\log y)^3$ term, which has a simple closed form [26].

Because coefficients in many of the non-rational enhancement functions grow excessively large at high powers of e^2 , we generally only provide here in print the first few terms for those series in analytic form. However, expansions relevant to the discussion section V B are given to as many orders as necessary. Additionally, the 8PN non-log term, for which no new coefficients could be extracted, is given in approximate numeric form to 20 decimals of precision. We indicate the highest *analytic* power of e^2 found for each PN order via a Greek constant shown at the end of each series. Note that this is in contrast to Paper I, where listed constants represented known numeric coefficients. Even though we can report here only a subset of the full analytic structure that we have discovered, our full results are published in a MATHEMATICA notebook on the Black Hole Perturbation Toolkit website [40] for easy retrieval.

We start with a second presentation of all of the flux terms up to and including 3PN, this time in our $\mathcal{J}(e)$ notation. These enhancement functions can be found by fitting; however, they are more easily derived by simply recasting the functions of Sec. III in terms of the Darwin eccentricity e using Eq. (4.38) of Paper I. Computing them in both ways allows for an independent check of our methodology. In either case, we find that $\tilde{\varphi}$, \tilde{F} , and $\tilde{\chi}$ remain the same functions,

just with the replacement $e_t \rightarrow e$. On the other hand, coefficients in $\tilde{\psi}$ are changed by the transformation, which is reflected in the subscript D (for Darwin eccentricity). Note that all terms in (5.1) through (5.7) can be expanded to arbitrary order in e^2 , using the techniques described earlier for summing the various enhancement functions. Hence, we only show a few terms in these cases (see [40]). We find

$$\mathcal{J}_0 = \frac{1}{(1-e^2)^2} \left(1 + \frac{7}{8}e^2 \right), \quad (5.1)$$

$$\mathcal{J}_1 = -\frac{1}{(1-e^2)^3} \left(\frac{1247}{336} + \frac{2777}{336}e^2 + \frac{5713}{2688}e^4 \right), \quad (5.2)$$

$$\mathcal{J}_{3/2} = 4\pi\tilde{\phi}(e), \quad (5.3)$$

$$\mathcal{J}_2 = \frac{1}{(1-e^2)^4} \left(-\frac{135431}{9072} - \frac{190087}{6048}e^2 + \frac{192133}{24192}e^4 + \frac{3499}{2304}e^6 \right) + \frac{10}{(1-e^2)^{5/2}} \left(1 + \frac{7}{8}e^2 \right), \quad (5.4)$$

$$\begin{aligned} \mathcal{J}_{5/2} &= -\frac{8191}{672}\pi\tilde{\psi}_D(e) \\ &= -\frac{8191}{672}\frac{\pi}{(1-e^2)^{9/2}} \left(1 + \frac{102121}{16382}e^2 + \frac{3557227}{524224}e^4 + \frac{6395111}{9436032}e^6 + \frac{5968651}{603906048}e^8 - \frac{59360743}{30195302400}e^{10} + \dots \right), \end{aligned} \quad (5.5)$$

$$\begin{aligned} \mathcal{J}_3 &= \frac{1}{(1-e^2)^5} \left[\frac{2017023341}{9979200} + \frac{3081414883}{2494800}e^2 + \frac{1949678087}{1900800}e^4 + \frac{621661339}{4435200}e^6 + \frac{29539919}{5677056}e^8 \right. \\ &\quad \left. - \sqrt{1-e^2} \left(\frac{379223}{5040} + \frac{138673}{630}e^2 - \frac{196073}{5760}e^4 - \frac{36405}{896}e^6 \right) \right] + \left(\frac{16}{3}\pi^2 - \frac{1712}{105}\gamma_E - \frac{116761}{3675} \right) \tilde{F}(e) \\ &\quad - \frac{1712}{105} \log \left(\frac{8(1-e^2)}{1+\sqrt{1-e^2}} \right) \tilde{F}(e) - \frac{1712}{105} \tilde{\chi}(e), \end{aligned} \quad (5.6)$$

$$\mathcal{J}_{3L} = -\frac{1}{(1-e^2)^5} \left(\frac{856}{105} + \frac{24503e^2}{420} + \frac{11663e^4}{280} + \frac{2461e^6}{1120} \right). \quad (5.7)$$

From this point, we present new coefficients found by fitting. We start with the 3.5PN enhancement function, which was computed to e^{30} .

$$\begin{aligned} \mathcal{J}_{7/2} &= \frac{\pi}{(1-e^2)^{11/2}} \left(-\frac{16285}{504} - \frac{370255}{1008}e^2 - \frac{11888119}{48384}e^4 + \frac{6476904953}{20901888}e^6 + \frac{8877357035}{167215104}e^8 + \frac{186159455101}{26754416640}e^{10} \right. \\ &\quad + \frac{34468729921289}{9631589990400}e^{12} + \frac{7790078031395741}{3775583276236800}e^{14} + \frac{319549718350556899}{241637329679155200}e^{16} + \frac{23734478429688515533}{26096831605348761600}e^{18} \\ &\quad + \frac{857752832161057782787}{1304841580267438080000}e^{20} + \frac{1662293559107552959945669}{3368231065863680163840000}e^{22} + \frac{208313298078191084760346703}{545653432669916186542080000}e^{24} \\ &\quad + \frac{7142452708941483674392066761043}{23607150111031253894556549120000}e^{26} + \frac{2263710549385314213293062077437587}{9254002843524251526666167255040000}e^{28} \\ &\quad \left. + \frac{1845877280291874535352833774291427}{9177523481181075894214380748800000}e^{30} + \dots \right). \end{aligned} \quad (5.8)$$

Next are the 4PN and 4PN log terms. The 4PN non-log series was found to e^{30} through eulerlog simplifications. We show the series up to e^{10} to illustrate some of its structure, which will be discussed in the next subsection. The remainder of the series can be found at [40].

$$\begin{aligned} \mathcal{J}_4 &= \frac{1}{(1-e^2)^6} \left[-\frac{323105549467}{3178375200} + \frac{232597\gamma_E}{4410} - \frac{1369\pi^2}{126} + \frac{39931 \log(2)}{294} - \frac{47385 \log(3)}{1568} + \left(-\frac{25591550692117}{12713500800} \right. \right. \\ &\quad \left. \left. + \frac{3482879\gamma_E}{4410} - \frac{22495\pi^2}{126} - \frac{744809 \log(2)}{490} + \frac{8684577 \log(3)}{3920} \right) e^2 + \left(-\frac{230437128487837}{25427001600} + \frac{34971299\gamma_E}{17640} \right. \right. \\ &\quad \left. \left. - \frac{259969\pi^2}{504} + \frac{1133219251 \log(2)}{17640} - \frac{9701228007 \log(3)}{501760} - \frac{3173828125 \log(5)}{301056} \right) e^4 + \left(-\frac{511692926097851}{50854003200} \right. \right. \\ &\quad \left. \left. + \frac{6578731\gamma_E}{7056} - \frac{89393\pi^2}{336} - \frac{28743092759 \log(2)}{45360} + \frac{4730808321 \log(3)}{501760} + \frac{314655859375 \log(5)}{1161216} \right) e^6 \right. \\ &\quad \left. + \left(-\frac{228428222760809}{67805337600} + \frac{2503623\gamma_E}{62720} - \frac{21495\pi^2}{1792} + \frac{3273460573169 \log(2)}{725760} + \frac{3963317295231 \log(3)}{2621440} \right) \right. \end{aligned}$$

$$\begin{aligned}
& - \frac{5065761265234375 \log(5)}{2080899072} - \frac{6297785676455 \log(7)}{14155776} \Big) e^8 + \left(- \frac{15338989354349}{11070259200} - \frac{246231168185717 \log(2)}{7938000} \right. \\
& - \frac{12237402512884383 \log(3)}{802816000} + \frac{6381944296484375 \log(5)}{520224768} + \frac{12620489342050037 \log(7)}{1327104000} \Big) e^{10} \\
& + \dots + \alpha_{30} e^{30} + \dots \Big]. \tag{5.9}
\end{aligned}$$

The 4PN log term, found earlier [39], revealed an exact, closed-form expression:

$$\mathcal{J}_{4L} = \frac{1}{(1-e^2)^6} \left(\frac{232597}{8820} + \frac{3482879e^2}{8820} + \frac{34971299e^4}{35280} + \frac{6578731e^6}{14112} + \frac{2503623e^8}{125440} \right). \tag{5.10}$$

The 4.5PN functions were both found to e^{30} . We give the non-log function to e^{10} in order to contrast it with \mathcal{J}_4 above, with the remainder posted at [40].

$$\begin{aligned}
\mathcal{J}_{9/2} = & \frac{\pi}{(1-e^2)^{13/2}} \left[\frac{265978667519}{745113600} - \frac{6848\gamma_E}{105} - \frac{13696 \log(2)}{105} + \left(\frac{119401899839}{19353600} - \frac{27713\gamma_E}{30} - \frac{36487 \log(2)}{210} \right. \right. \\
& - \left. \frac{234009 \log(3)}{140} \right) e^2 + \left(\frac{38291634777373}{2167603200} - \frac{1474139\gamma_E}{840} - \frac{6556639 \log(2)}{168} + \frac{2106081 \log(3)}{112} \right) e^4 \\
& + \left(\frac{15381024734595431}{1287556300800} - \frac{71788333\gamma_E}{120960} + \frac{47822794963 \log(2)}{120960} - \frac{172932651 \log(3)}{1792} - \frac{5224609375 \log(5)}{48384} \right) e^6 \\
& + \left(\frac{3913633755471997}{3139184885760} - \frac{513707\gamma_E}{27648} - \frac{2513356038497 \log(2)}{967680} - \frac{17373530187 \log(3)}{71680} + \frac{496337890625 \log(5)}{387072} \right) e^8 \\
& + \left(\frac{1983010121518334771}{2354388664320000} - \frac{690257\gamma_E}{55296000} + \frac{5129311678694857 \log(2)}{387072000} + \frac{346105863017991 \log(3)}{57344000} \right. \\
& \left. - \frac{87339794921875 \log(5)}{12386304} - \frac{507989081563901 \log(7)}{221184000} \right) e^{10} + \dots + \beta_{30} e^{30} + \dots \Big], \tag{5.11}
\end{aligned}$$

$$\begin{aligned}
\mathcal{J}_{9/2L} = & \frac{\pi}{(1-e^2)^{13/2}} \left(- \frac{3424}{105} - \frac{27713}{60} e^2 - \frac{1474139}{1680} e^4 - \frac{71788333}{241920} e^6 - \frac{513707}{55296} e^8 - \frac{690257}{110592000} e^{10} - \frac{32944979}{9289728000} e^{12} \right. \\
& + \frac{1896198253}{14566293504000} e^{14} + \frac{217366002683}{699182088192000} e^{16} + \frac{20237480138479}{1812279972593664000} e^{18} - \frac{1186535077588513}{181227997259366400000} e^{20} \\
& - \frac{570980043986842753}{350857402694133350400000} e^{22} - \frac{6584105389810998751}{25261732993977601228800000} e^{24} - \frac{3047031016950659382647}{68307726015715433722675200000} e^{26} \\
& \left. - \frac{175631935156003401313237}{13388314299080225009644339200000} e^{28} - \frac{80704977292116623135976991}{12852781727117016009258565632000000} e^{30} + \dots \right). \tag{5.12}
\end{aligned}$$

Analytic coefficients were also found to e^{30} in the 5PN non-log series. There is no novel behavior in the appearance of γ_E and π^2 in the series, so we truncate at e^8 and leave the rest to [40].

$$\begin{aligned}
\mathcal{J}_5 = & \frac{1}{(1-e^2)^7} \left[- \frac{2500861660823683}{2831932303200} + \frac{916628467\gamma_E}{7858620} - \frac{424223\pi^2}{6804} - \frac{83217611 \log(2)}{1122660} + \frac{47385 \log(3)}{196} \right. \\
& + \left(- \frac{7848030223872703}{471988717200} + \frac{769099141\gamma_E}{523908} - \frac{2387269\pi^2}{2268} + \frac{2778275573 \log(2)}{124740} - \frac{33084207 \log(3)}{5390} \right. \\
& \left. - \frac{76708984375 \log(5)}{25147584} \right) e^2 + \left(- \frac{60115129871947373}{1373058086400} - \frac{453258311\gamma_E}{476280} - \frac{4569965\pi^2}{2268} - \frac{8765389513 \log(2)}{21384} \right. \\
& \left. - \frac{3015086409 \log(3)}{2759680} + \frac{72979638671875 \log(5)}{402361344} \right) e^4 + \left(\frac{51952994948318117}{3624873348096} - \frac{373576122307\gamma_E}{31434480} + \frac{43547141\pi^2}{27216} \right. \\
& + \frac{457831837310951 \log(2)}{94303440} + \frac{10321124212899 \log(3)}{5519360} - \frac{5005044628796875 \log(5)}{1810626048} - \frac{152212635349397 \log(7)}{295612416} \Big) e^6 \\
& + \left(\frac{8413909247102002313}{161105482137600} - \frac{232447680943\gamma_E}{37255680} + \frac{49944247\pi^2}{32256} - \frac{44427069728132087 \log(2)}{823011840} - \right. \\
& \left. \frac{1262436103060623 \log(3)}{44154880} + \frac{277340233759765625 \log(5)}{12875563008} + \frac{82923917976541537 \log(7)}{4729798656} \right) e^8 + \dots + \gamma_{30} e^{30} + \dots \Big]. \tag{5.13}
\end{aligned}$$

The 5PN log flux revealed a closed-form representation with a two polynomial structure reminiscent of the 2PN flux. Note the recurrence of the 3PN log term (see [26]).

$$\mathcal{J}_{5L} = \frac{1}{(1-e^2)^7} \left(\frac{4119951667}{15717240} + \frac{1977018931}{1047816} e^2 - \frac{1472497511}{952560} e^4 - \frac{433137913057}{62868960} e^6 - \frac{202342374943}{74511360} e^8 - \frac{7349401019}{74511360} e^{10} \right) - \frac{25}{(1-e^2)^{11/2}} \left(\frac{856}{105} + \frac{24503e^2}{420} + \frac{11663e^4}{280} + \frac{2461e^6}{1120} \right). \quad (5.14)$$

Like those at 4.5PN non-log and log terms, the two 5.5PN enhancement functions were obtained through e^{30} . The 5.5PN non-log has a structure that parallels that of the 4.5PN non-log flux, so it is only given to e^8 (see [40]).

$$\begin{aligned} \mathcal{J}_{11/2} = & \frac{1}{(1-e^2)^{15/2}} \left[\frac{8399309750401}{101708006400} + \frac{177293\gamma_E}{1176} + \frac{8521283 \log(2)}{17640} - \frac{142155 \log(3)}{784} + \left(-\frac{317038110775093}{31294771200} \right. \right. \\ & + \frac{64081361\gamma_E}{11760} - \frac{406889101 \log(2)}{35280} + \frac{119451753 \log(3)}{7840} \left. \right) e^2 + \left(-\frac{348610408725721199}{3254656204800} + \frac{10614822977\gamma_E}{376320} \right. \\ & + \frac{224456603713 \log(2)}{376320} - \frac{38840680413 \log(3)}{250880} - \frac{15869140625 \log(5)}{150528} \left. \right) e^4 + \left(-\frac{27027476102569882391}{117167623372800} \right. \\ & + \frac{74351130037\gamma_E}{2257920} - \frac{9038099531309 \log(2)}{1354752} - \frac{13841114031 \log(3)}{100352} + \frac{24891232421875 \log(5)}{8128512} \left. \right) e^6 \\ & + \left(-\frac{2224416660039631007669}{14997455791718400} + \frac{401363859989\gamma_E}{48168960} + \frac{163924038199663 \log(2)}{2949120} + \frac{193784040880587 \log(3)}{9175040} \right. \\ & \left. - \frac{32000395138671875 \log(5)}{1040449536} - \frac{44084499735185 \log(7)}{7077888} \right) e^8 + \dots + \delta_{30} e^{30} + \dots \Big], \quad (5.15) \end{aligned}$$

$$\begin{aligned} \mathcal{J}_{11/2L} = & \frac{\pi}{(1-e^2)^{15/2}} \left(\frac{177293}{2352} + \frac{64081361}{23520} e^2 + \frac{10614822977}{752640} e^4 + \frac{74351130037}{4515840} e^6 + \frac{401363859989}{96337920} e^8 \right. \\ & + \frac{415995121057}{3715891200} e^{10} - \frac{7209622999493}{8323596288000} e^{12} + \frac{72341367473941}{349591044096000} e^{14} - \frac{42609390600435763}{1879401453060096000} e^{16} \\ & - \frac{100722749765702921}{101487678465245184000} e^{18} + \frac{12431692376218945133}{81190142772196147200000} e^{20} - \frac{87071794412050090903}{6549338183623822540800000} e^{22} \\ & - \frac{24657404147085482364377}{377241879376321783500800000} e^{24} + \frac{1024340334562524085072459}{1275077552293354762823270400000} e^{26} \\ & \left. + \frac{6248139326602860647729211263}{5536582897835022280911382118400000} e^{28} + \frac{10800846845298064086150500419}{18455276326116740936371273728000000} e^{30} + \dots \right). \quad (5.16) \end{aligned}$$

The 6PN order reveals the first significant increase in complexity, limiting output in the non-log series to e^{20} even with our new methods. Coefficients are given to e^{12} to aid the discussion in Sec. VB, but a few are skipped in the middle of the 6PN non-log series for the sake of brevity. The 6PN log term, meanwhile, was found to e^{30} , but is also abbreviated here. All of the now-known coefficients for both of these series are available at [40].

$$\begin{aligned} \mathcal{J}_6 = & \frac{1}{(1-e^2)^8} \left[\frac{2067586193789233570693}{602387400044430000} - \frac{246137536815857\gamma_E}{157329572400} + \frac{1465472\gamma_E^2}{11025} + \frac{3803225263\pi^2}{10478160} - \frac{27392\gamma_E\pi^2}{315} \right. \\ & - \frac{256\pi^4}{45} - \frac{271272899815409 \log(2)}{157329572400} + \frac{5861888\gamma_E \log(2)}{11025} - \frac{54784}{315} \pi^2 \log(2) + \frac{5861888 \log^2(2)}{11025} \\ & - \frac{437114506833 \log(3)}{789268480} - \frac{37744140625 \log(5)}{260941824} - \frac{27392\zeta(3)}{105} + \left(\frac{333496126867093189441241}{2409549600177720000} \right. \\ & - \frac{7595864167160341\gamma_E}{157329572400} + \frac{37312291\gamma_E^2}{11025} + \frac{131859072299\pi^2}{10478160} - \frac{697426\gamma_E\pi^2}{315} - \frac{6518\pi^4}{45} - \frac{753377050209181 \log(2)}{6293182896} \\ & + \frac{7304462\gamma_E \log(2)}{2205} - \frac{68266}{63} \pi^2 \log(2) - \frac{19841117 \log^2(2)}{11025} - \frac{1908385569124767 \log(3)}{27624396800} + \frac{25038963\gamma_E \log(3)}{2450} \\ & - \frac{234009}{70} \pi^2 \log(3) + \frac{25038963 \log(2) \log(3)}{2450} + \frac{25038963 \log^2(3)}{4900} + \frac{4771622294921875 \log(5)}{115075344384} - \frac{697426\zeta(3)}{105} \left. \right) e^2 \\ & + \left(\frac{11732182856513046341196869}{12850931200947840000} - \frac{101582265565497851\gamma_E}{419545526400} + \frac{48268984\gamma_E^2}{3675} + \frac{2007227812021\pi^2}{27941760} \right. \end{aligned}$$

$$\begin{aligned}
& - \frac{902224\gamma_E\pi^2}{105} - \frac{8432\pi^4}{15} - \frac{62869385779677563 \log(2)}{419545526400} + \frac{3516949616\gamma_E \log(2)}{11025} - \frac{32868688}{315}\pi^2 \log(2) \\
& + \frac{926636264 \log^2(2)}{1575} + \frac{288069901518860361 \log(3)}{160723763200} - \frac{1276987113\gamma_E \log(3)}{9800} + \frac{11934459}{280}\pi^2 \log(3) \\
& - \frac{1276987113 \log(2) \log(3)}{9800} - \frac{1276987113 \log^2(3)}{19600} - \frac{9599818019775390625 \log(5)}{7364822040576} - \frac{3669865047185939 \log(7)}{16700276736} \\
& - \frac{902224\zeta(3)}{35} e^4 + \dots + \left(\frac{1102884951466368489130807}{10544353805905920000} + \frac{342273999229759\gamma_E}{57373747200} + \frac{1614309\gamma_E^2}{31360} \right. \\
& + \frac{32395236497\pi^2}{16558080} - \frac{15087\gamma_E\pi^2}{448} - \frac{141\pi^4}{64} - \frac{3767593808715133006785437 \log(2)}{411917425920000} - \frac{27170243004666463\gamma_E \log(2)}{158760000} \\
& + \frac{253927504716509\pi^2 \log(2)}{4536000} - \frac{94122888541066079 \log^2(2)}{317520000} + \frac{6158909116569246725891349 \log(3)}{5657476464640000} \\
& - \frac{84905458917700797\gamma_E \log(3)}{1003520000} + \frac{793508961847671\pi^2 \log(3)}{28672000} - \frac{176618348868400317 \log(2) \log(3)}{1003520000} \\
& - \frac{84905458917700797 \log^2(3)}{2007040000} - \frac{2860433896932411829109375 \log(5)}{9898320822534144} + \frac{11948216650390625\gamma_E \log(5)}{130056192} \\
& - \frac{558327880859375\pi^2 \log(5)}{18579456} + \frac{11948216650390625 \log(2) \log(5)}{130056192} + \frac{11948216650390625 \log^2(5)}{260112384} \\
& + \frac{24952742409203475686255233 \log(7)}{8657423459942400} + \frac{54354831727337407\gamma_E \log(7)}{1658880000} - \frac{3555923570947307\pi^2 \log(7)}{331776000} \\
& + \frac{54354831727337407 \log(2) \log(7)}{1658880000} + \frac{54354831727337407 \log^2(7)}{3317760000} - \frac{45261\zeta(3)}{448} \Big) e^{10} \\
& + \left(\frac{965874068977331961500021}{8392444865925120000} - \frac{11778703354456943\gamma_E}{852409958400} + \frac{815219098163\pi^2}{170311680} \right. \\
& + \frac{4370148427543824812401338563 \log(2)}{46605514475520000} + \frac{15544521547964903\gamma_E \log(2)}{12757500} - \frac{145275902317429\pi^2 \log(2)}{364500} \\
& + \frac{420172500588128243 \log^2(2)}{178605000} - \frac{3268367789575842149871375567 \log(3)}{90519623434240000} + \frac{2324949929559348129\gamma_E \log(3)}{4014080000} \\
& - \frac{21728504014573347\pi^2 \log(3)}{114688000} + \frac{939690587607417837 \log(2) \log(3)}{802816000} + \frac{2324949929559348129 \log^2(3)}{8028160000} + \\
& 191286506617120840992788490625 \log(5) - \frac{1664837216064453125\gamma_E \log(5)}{4682022912} + \frac{77796131591796875\pi^2 \log(5)}{668860416} \\
& - \frac{1664837216064453125 \log(2) \log(5)}{4682022912} - \frac{1664837216064453125 \log^2(5)}{9364045824} - \frac{459130554615555174602630946209 \log(7)}{24933379564634112000} \\
& - \frac{1032741802819410733\gamma_E \log(7)}{2211840000} + \frac{67562547847998833\pi^2 \log(7)}{442368000} - \frac{1032741802819410733 \log(2) \log(7)}{2211840000} \\
& - \frac{1032741802819410733 \log^2(7)}{4423680000} - \frac{5720393206911557758236103 \log(11)}{4579133069721600} \Big) e^{12} + \dots + \epsilon_{20}e^{20} + \dots \Big], \quad (5.17)
\end{aligned}$$

$$\begin{aligned}
\mathcal{J}_{6L} = & \frac{1}{(1-e^2)^8} \left[- \frac{246137536815857}{314659144800} + \frac{1465472\gamma_E}{11025} - \frac{13696\pi^2}{315} + \frac{2930944 \log(2)}{11025} + \left(- \frac{7595864167160341}{314659144800} \right. \right. \\
& + \frac{37312291\gamma_E}{11025} - \frac{348713\pi^2}{315} + \frac{3652231 \log(2)}{2205} + \frac{25038963 \log(3)}{4900} \Big) e^2 + \left(- \frac{101582265565497851}{839091052800} + \frac{48268984\gamma_E}{3675} \right. \\
& - \frac{451112\pi^2}{105} + \frac{1758474808 \log(2)}{11025} - \frac{1276987113 \log(3)}{19600} \Big) e^4 + \left(- \frac{188707966764313411}{1258636579200} + \frac{105365147\gamma_E}{8820} \right. \\
& - \frac{984721\pi^2}{252} - \frac{712154281537 \log(2)}{396900} + \frac{120161983437 \log(3)}{313600} + \frac{559033203125 \log(5)}{1016064} \Big) e^6 \\
& + \left(- \frac{1036935631457042173}{40276370534400} + \frac{42578831\gamma_E}{17640} - \frac{397933\pi^2}{504} + \frac{1596888808397 \log(2)}{113400} + \frac{4849120691469 \log(3)}{2508800} \right. \\
& - \frac{59816552734375 \log(5)}{8128512} \Big) e^8 + \left(\frac{342273999229759}{114747494400} + \frac{1614309\gamma_E}{31360} - \frac{15087\pi^2}{896} - \frac{27170243004666463 \log(2)}{317520000} \right.
\end{aligned}$$

$$\begin{aligned}
& - \frac{84905458917700797 \log(3)}{2007040000} + \frac{11948216650390625 \log(5)}{260112384} + \frac{54354831727337407 \log(7)}{3317760000} \Big) e^{10} \\
& + \left(- \frac{11778703354456943}{1704819916800} + \frac{15544521547964903 \log(2)}{25515000} + \frac{2324949929559348129 \log(3)}{8028160000} \right. \\
& \left. - \frac{1664837216064453125 \log(5)}{9364045824} - \frac{1032741802819410733 \log(7)}{4423680000} \right) e^{12} + \dots + \zeta_{30} e^{30} + \dots \Big], \tag{5.18}
\end{aligned}$$

The 6PN \log^2 flux yielded another closed form expression (for its origin see [26])

$$\mathcal{J}_{6L^2} = \frac{1}{(1-e^2)^8} \left(\frac{366368}{11025} + \frac{37312291e^2}{44100} + \frac{12067246e^4}{3675} + \frac{105365147e^6}{35280} + \frac{42578831e^8}{70560} + \frac{1614309e^{10}}{125440} \right). \tag{5.19}$$

Mirroring 4.5PN and 5.5PN in appearance, analysis of the 6.5PN non-log flux yielded analytic coefficients to e^{28} (abbreviated here with the rest found at [40]). The 6.5PN log series was extracted to e^{30} .

$$\begin{aligned}
\mathcal{J}_{13/2} = & \frac{1}{(1-e^2)^{17/2}} \left[- \frac{81605095538444363}{20138185267200} + \frac{300277177\gamma_E}{436590} - \frac{42817273 \log(2)}{71442} + \frac{142155 \log(3)}{98} \right. \\
& + \left(- \frac{234251633966628833}{1917922406400} + \frac{3018730571\gamma_E}{249480} + \frac{2945961630581 \log(2)}{15717240} - \frac{200620071 \log(3)}{4312} \right. \\
& \left. - \frac{383544921875 \log(5)}{12573792} \right) e^2 + \left(- \frac{774717636162954505499}{1288843857100800} - \frac{1025646313\gamma_E}{3104640} - \frac{1054969026721721 \log(2)}{251475840} \right. \\
& \left. - \frac{125742420117 \log(3)}{689920} + \frac{199777099609375 \log(5)}{100590336} \right) e^4 + \left(- \frac{3686697161827337895751}{29827529264332800} - \frac{547729534754263\gamma_E}{2586608640} \right. \\
& + \frac{118655627259703271 \log(2)}{2011806720} + \frac{69674180291811 \log(3)}{2759680} - \frac{61926330507109375 \log(5)}{1810626048} \\
& \left. - \frac{1065488447445779 \log(7)}{147806208} \right) e^6 + \dots + \eta_{28} e^{28} + \dots \Big], \tag{5.20}
\end{aligned}$$

$$\begin{aligned}
\mathcal{J}_{13/2L} = & \frac{\pi}{(1-e^2)^{17/2}} \left(\frac{300277177}{873180} + \frac{3018730571}{498960} e^2 - \frac{1025646313}{6209280} e^4 - \frac{547729534754263}{5173217280} e^6 - \frac{1847568691294327}{13168189440} e^8 \right. \\
& - \frac{150836673548029393}{4213820620800} e^{10} - \frac{341056100428493993}{151697542348800} e^{12} - \frac{900692084654430303761}{1308239605216051200} e^{14} \\
& - \frac{183817754019571452481}{478441912764727296} e^{16} - \frac{1369950195790953661052617}{5651595094533341184000} e^{18} - \frac{60937088128013175521329153}{369083761275646771200000} e^{20} \\
& - \frac{2076214844718290480358259887751}{17506380964826477651558400000} e^{22} - \frac{67058838175907561436011530774049}{756275657680503834547322880000} e^{24} \\
& - \frac{399586784196479229606707351966520311}{5842769652480235338902745907200000} e^{26} - \frac{19706198618409033215085911333142483997}{364376361963767403862480335667200000} e^{28} \\
& \left. - \frac{1333103852525373905617630701770154129101}{30538209383630030037998351941632000000} e^{30} + \dots \right). \tag{5.21}
\end{aligned}$$

The 7PN non-log series, of similar complexity to its 6PN counterpart, was extracted to e^{12} . Only the first 3 coefficients are listed here. The 7PN log term was obtained to e^{26} , but its presentation here is truncated at e^{14} . See [40] for complete expressions.

$$\begin{aligned}
\mathcal{J}_7 = & \frac{1}{(1-e^2)^9} \left[\frac{58327313257446476199371189}{8332222517414555760000} + \frac{9640384387033067\gamma_E}{17896238860500} - \frac{52525903\gamma_E^2}{154350} + \frac{2621359845833\pi^2}{2383781400} \right. \\
& + \frac{531077\gamma_E\pi^2}{6615} - \frac{9523\pi^4}{945} + \frac{1940223250751339 \log(2)}{17896238860500} - \frac{471188717\gamma_E \log(2)}{231525} + \frac{128223}{245} \pi^2 \log(2) \\
& - \frac{5811697 \log^2(2)}{2450} - \frac{6136997968378863 \log(3)}{1256910054400} + \frac{1848015\gamma_E \log(3)}{2744} - \frac{142155}{392} \pi^2 \log(3) + \frac{1848015 \log(2) \log(3)}{2744} \\
& + \frac{1848015 \log^2(3)}{5488} + \frac{9926708984375 \log(5)}{5088365568} + \frac{531077\zeta(3)}{2205} + \left(- \frac{217658436746027815895102341}{1666444503482911152000} \right. \\
& \left. + \frac{24231077015148314777\gamma_E}{143169910884000} - \frac{2214256717\gamma_E^2}{92610} - \frac{1329680222711\pi^2}{866829600} + \frac{14572037\gamma_E\pi^2}{1323} + \frac{210017\pi^4}{945} \right)
\end{aligned}$$

$$\begin{aligned}
& - \frac{11466432970124391527 \log(2)}{143169910884000} + \frac{8341589759 \gamma_E \log(2)}{231525} - \frac{69704909 \pi^2 \log(2)}{2205} + \frac{63780712447 \log^2(2)}{463050} \\
& + \frac{2351107897519100859 \log(3)}{3591171584000} - \frac{939847941 \gamma_E \log(3)}{9800} + \frac{9620613}{280} \pi^2 \log(3) - \frac{939847941 \log(2) \log(3)}{9800} \\
& - \frac{939847941 \log^2(3)}{19600} - \frac{1612267989365234375 \log(5)}{6981237559296} - \frac{611078988636949 \log(7)}{21201523200} + \frac{14572037 \zeta(3)}{441} \Big) e^2 \\
& + \left(- \frac{130192781785212682155024739573}{33328890069658223040000} + \frac{591633756214144946231 \gamma_E}{286339821768000} - \frac{763796786629 \gamma_E^2}{3704400} \right. \\
& - \frac{86202827232472 \pi^2}{297972675} + \frac{5789871557 \gamma_E \pi^2}{52920} + \frac{6673217 \pi^4}{1512} + \frac{4393870365431735509303 \log(2)}{286339821768000} \\
& - \frac{117429592367 \gamma_E \log(2)}{24696} + \frac{19166514113 \pi^2 \log(2)}{10584} - \frac{10950400503703 \log^2(2)}{1234800} - \frac{42089890286054028933 \log(3)}{3093932441600} \\
& + \frac{4964131679733 \gamma_E \log(3)}{4390400} - \frac{49938060789 \pi^2 \log(3)}{125440} + \frac{4964131679733 \log(2) \log(3)}{4390400} + \frac{4964131679733 \log^2(3)}{8780800} \\
& - \frac{50857646229982421875 \log(5)}{1172847909961728} + \frac{1031494140625 \gamma_E \log(5)}{1580544} - \frac{79345703125 \pi^2 \log(5)}{225792} \\
& + \frac{1031494140625 \log(2) \log(5)}{1580544} + \frac{1031494140625 \log^2(5)}{3161088} + \frac{18836032355690667229 \log(7)}{4070692454400} + \frac{5789871557 \zeta(3)}{17640} \Big) e^4 \\
& + \dots + \theta_{12} e^{12} + \dots \Big], \tag{5.22}
\end{aligned}$$

$$\begin{aligned}
\mathcal{J}_{7L} = & \frac{1}{(1 - e^2)^9} \left[\frac{9640384387033067}{35792477721000} - \frac{52525903 \gamma_E}{154350} + \frac{531077 \pi^2}{13230} - \frac{471188717 \log(2)}{463050} + \frac{1848015 \log(3)}{5488} \right. \\
& + \left(\frac{24231077015148314777}{286339821768000} - \frac{2214256717 \gamma_E}{92610} + \frac{14572037 \pi^2}{2646} + \frac{8341589759 \log(2)}{463050} - \frac{939847941 \log(3)}{19600} \right) e^2 \\
& + \left(\frac{591633756214144946231}{572679643536000} - \frac{763796786629 \gamma_E}{3704400} + \frac{5789871557 \pi^2}{105840} - \frac{117429592367 \log(2)}{49392} \right. \\
& + \frac{4964131679733 \log(3)}{8780800} + \frac{1031494140625 \log(5)}{3161088} \Big) e^4 + \left(\frac{7068212226017284341287}{2290718574144000} - \frac{824747159647 \gamma_E}{1852200} \right. \\
& + \frac{6687480911 \pi^2}{52920} + \frac{482678846963689 \log(2)}{16669800} + \frac{109318137597 \log(3)}{627200} - \frac{580527388671875 \log(5)}{42674688} \Big) e^6 \\
& + \left(\frac{1118293348517845456727}{366514971863040} - \frac{3296625810013 \gamma_E}{11854080} + \frac{27848763749 \pi^2}{338688} - \frac{150747095221023577 \log(2)}{533433600} \right. \\
& - \frac{242530132831033581 \log(3)}{2247884800} + \frac{3529852121076171875 \log(5)}{21849440256} + \frac{573098496557405 \log(7)}{21233664} \Big) e^8 \\
& + \left(\frac{7417800287709479830427}{7330299437260800} - \frac{515546659387 \gamma_E}{11854080} + \frac{4476597491 \pi^2}{338688} + \frac{34281927681591020089 \log(2)}{13335840000} \right. \\
& + \frac{11043010597723065117 \log(3)}{8028160000} - \frac{2515592654376953125 \log(5)}{2427715584} - \frac{33276227221291377337 \log(7)}{39813120000} \Big) e^{10} \\
& + \left(\frac{782647393237829745047}{2443433145753600} - \frac{8161170019 \gamma_E}{10536960} + \frac{72242227 \pi^2}{301056} - \frac{24632208831281134768831 \log(2)}{960180480000} \right. \\
& - \frac{13240749939950955181941 \log(3)}{1798307840000} + \frac{13741105065468587890625 \log(5)}{3146319396864} + \frac{222041600754634101785281 \log(7)}{22932357120000} \Big) e^{12} \\
& + \left(\frac{1679007616758134752753}{6515821722009600} + \frac{79294797830738769387229 \log(2)}{367569090000} - \frac{202498419750717826393947 \log(3)}{22029271040000} \right. \\
& - \frac{176421957727012978515625 \log(5)}{19271206305792} - \frac{122463544084536896035417 \log(7)}{1911029760000} \Big) e^{14} + \dots + \kappa_{26} e^{26} + \dots \Big]. \tag{5.23}
\end{aligned}$$

Like its 6PN counterpart, the \log^2 piece was also found to have a closed-form expression (see [34])

$$\mathcal{J}_{7L^2} = \frac{1}{(1-e^2)^9} \left(\frac{52525903}{617400} + \frac{2214256717}{370440} e^2 + \frac{763796786629}{14817600} e^4 + \frac{824747159647}{7408800} e^6 + \frac{3296625810013}{47416320} e^8 \right. \\ \left. + \frac{515546659387}{47416320} e^{10} + \frac{8161170019}{42147840} e^{12} \right). \quad (5.24)$$

The 7.5PN half-integer series presented difficulties, allowing us to find analytic coefficients only through e^{12} . The corresponding log and \log^2 terms were found to e^{26} and e^{28} , respectively.

$$\mathcal{J}_{15/2} = \frac{\pi}{(1-e^2)^{19/2}} \left[\frac{51603801120086143145449}{8567287467298560000} - \frac{3025414963439009\gamma_E}{559394035200} + \frac{5861888\gamma_E^2}{11025} - \frac{1465472\pi^2}{11025} \right. \\ - \frac{1999998476702377 \log(2)}{5034546316800} + \frac{23447552\gamma_E \log(2)}{11025} + \frac{23447552 \log^2(2)}{11025} - \frac{1311343520499 \log(3)}{394634240} \\ - \frac{188720703125 \log(5)}{130470912} - \frac{109568\zeta(3)}{105} + \left(\frac{2662696956467596386499309}{3426914986919424000} - \frac{349953536858546087\gamma_E}{1118788070400} \right. \\ \left. + \frac{50616029\gamma_E^2}{2205} - \frac{50616029\pi^2}{8820} - \frac{11140310485001952479 \log(2)}{10069092633600} + \frac{336165538\gamma_E \log(2)}{11025} \right. \\ - \frac{1911983 \log^2(2)}{11025} - \frac{12592554481394127 \log(3)}{27624396800} + \frac{75116889\gamma_E \log(3)}{1225} + \frac{75116889 \log(2) \log(3)}{1225} \\ \left. + \frac{75116889 \log^2(3)}{2450} + \frac{7153146044921875 \log(5)}{16439334912} - \frac{946094\zeta(3)}{21} \right) e^2 + \left(\frac{1215046582634472109846437257}{126532245670871040000} \right. \\ - \frac{11416899892367577827\gamma_E}{4130909798400} + \frac{7015042729\gamma_E^2}{44100} - \frac{7015042729\pi^2}{176400} + \frac{974649950407627431787 \log(2)}{161105482137600} \\ \left. + \frac{57310041769\gamma_E \log(2)}{22050} + \frac{5883446467 \log^2(2)}{1260} + \frac{15692774935495349169 \log(3)}{883980697600} - \frac{4281662673\gamma_E \log(3)}{4900} \right. \\ - \frac{4281662673 \log(2) \log(3)}{4900} - \frac{4281662673 \log^2(3)}{9800} - \frac{56175438510986328125 \log(5)}{3682411020288} - \frac{25689055330301573 \log(7)}{8350138368} \\ \left. - \frac{65561147\zeta(3)}{210} \right) e^4 + \left(\frac{565749089288149621030397977099}{17765127292190294016000} - \frac{3720660313410463236349\gamma_E}{579979735695360} + \frac{372612960091\gamma_E^2}{1270080} \right. \\ - \frac{372612960091\pi^2}{5080320} - \frac{1787089659108846763543 \log(2)}{5114459750400} - \frac{2035608947081\gamma_E \log(2)}{64800} - \frac{80645525885093 \log^2(2)}{1270080} \\ - \frac{642174379247781899307 \log(3)}{1767961395200} + \frac{454231827783\gamma_E \log(3)}{78400} + \frac{454231827783 \log(2) \log(3)}{78400} \\ \left. + \frac{454231827783 \log^2(3)}{156800} + \frac{60188792123471152140625 \log(5)}{463983788556288} + \frac{2795166015625\gamma_E \log(5)}{254016} \right. \\ \left. + \frac{2795166015625 \log(2) \log(5)}{254016} + \frac{2795166015625 \log^2(5)}{508032} + \frac{1421510488851228906067 \log(7)}{6763612078080} \right. \\ \left. - \frac{3482364113\zeta(3)}{6048} \right) e^6 + \dots + \lambda_{12} e^{12} \Big], \quad (5.25)$$

$$\mathcal{J}_{15/2L} = \frac{\pi}{(1-e^2)^{19/2}} \left[-\frac{3025414963439009}{1118788070400} + \frac{5861888\gamma_E}{11025} + \frac{11723776 \log(2)}{11025} + \left(-\frac{349953536858546087}{2237576140800} \right. \right. \\ \left. + \frac{50616029\gamma_E}{2205} + \frac{168082769 \log(2)}{11025} + \frac{75116889 \log(3)}{2450} \right) e^2 + \left(-\frac{11416899892367577827}{8261819596800} + \frac{7015042729\gamma_E}{44100} \right. \\ \left. + \frac{57310041769 \log(2)}{44100} - \frac{4281662673 \log(3)}{9800} \right) e^4 + \left(-\frac{3720660313410463236349}{1159959471390720} + \frac{372612960091\gamma_E}{1270080} \right. \\ - \frac{2035608947081 \log(2)}{129600} + \frac{454231827783 \log(3)}{156800} + \frac{2795166015625 \log(5)}{508032} \Big) e^6 + \left(-\frac{855337222347819322823827}{494916041126707200} \right. \\ \left. + \frac{8066792325467\gamma_E}{50803200} + \frac{7496582286172507 \log(2)}{50803200} + \frac{6992405846343 \log(3)}{250880} - \frac{47517822265625 \log(5)}{580608} \right) e^8 \\ \left. + \dots + \xi_{26} e^{26} + \dots \right], \quad (5.26)$$

$$\begin{aligned}
\mathcal{J}_{15/2L^2} = & \frac{\pi}{(1-e^2)^{19/2}} \left(\frac{1465472}{11025} + \frac{50616029}{8820}e^2 + \frac{7015042729}{176400}e^4 + \frac{372612960091}{5080320}e^6 + \frac{8066792325467}{203212800}e^8 \right. \\
& + \frac{438339815188777}{81285120000}e^{10} + \frac{27165778367659}{325140480000}e^{12} + \frac{139559840953}{169940090880000}e^{14} - \frac{138994608139273}{73414119260160000}e^{16} \\
& - \frac{510325343998375097}{190289397122334720000}e^{18} + \frac{29294767139126946059}{19028939712233472000000}e^{20} - \frac{160261051102927034773}{1473601091315360071680000}e^{22} \\
& - \frac{144909050598554594415739}{2652481964367648129024000000}e^{24} - \frac{3780135848816146128183067}{1434462246330024108176179200000}e^{26} \\
& \left. + \frac{347794649410341565383017707}{281154600280684725202531123200000}e^{28} + \dots \right). \tag{5.27}
\end{aligned}$$

The 8PN non-log flux was the least successful term to analyze and allowed only confirmation of the (known) circular orbit limit [12]. Numeric coefficients were obtained to e^{10} , which we present here. The 8PN log function yielded coefficients to e^{18} . We list these here to e^6 with the remainder given at [40].

$$\begin{aligned}
\mathcal{J}_8 \approx & \frac{1}{(1-e^2)^{10}} \left(-\frac{2206020140875740874945597498877}{63104087235639138048360000} + \frac{17328950668070007334987\gamma_E}{1084297320079974000} - \frac{3428849385499\gamma_E^2}{2723011830} \right. \\
& - \frac{18584197930153871\pi^2}{4247898454800} + \frac{1397063663\gamma_E\pi^2}{1178793} + \frac{2192471\pi^4}{25515} - \frac{4773986555637567504053 \log(2)}{1084297320079974000} \\
& + \frac{15332591650681\gamma_E \log(2)}{6807529575} - \frac{11366135381}{5893965}\pi^2 \log(2) + \frac{106165554403193 \log^2(2)}{13615059150} + \frac{8479423463263174971 \log(3)}{213674709248000} \\
& - \frac{1848015\gamma_E \log(3)}{343} + \frac{142155}{49}\pi^2 \log(3) - \frac{1848015 \log(2) \log(3)}{343} - \frac{1848015 \log^2(3)}{686} - \frac{83415474560546875 \log(5)}{8477217036288} \\
& - \frac{2025852318599963 \log(7)}{2948939136000} + \frac{1397063663\zeta(3)}{392931} - 1954977.501298132062640986690e^2 - \\
& 26349959.944946765641790484057e^4 - 87126977.786788602494976694986e^6 - \\
& \left. 83445624.027185442658036338727e^8 - 3243044.237540247549987011144e^{10} + \dots \right), \tag{5.28}
\end{aligned}$$

$$\begin{aligned}
\mathcal{J}_{8L} = & \frac{1}{(1-e^2)^{10}} \left[\frac{17254929304352547776587}{2168594640159948000} - \frac{3428849385499\gamma_E}{2723011830} + \frac{1397063663\pi^2}{2357586} + \frac{15332591650681 \log(2)}{13615059150} \right. \\
& - \frac{1848015 \log(3)}{686} + \left(\frac{6902005678706412730657}{26772773335308000} - \frac{3056423284787\gamma_E}{605113740} + \frac{8584514299\pi^2}{523908} \right. \\
& \left. - \frac{4058693142384893 \log(2)}{9076706100} + \frac{2504263499487 \log(3)}{16601200} + \frac{602549072265625 \log(5)}{8713637856} \right) e^2 \\
& + \left(\frac{20464697512527803859881}{35697031113744000} + \frac{5591213449564669\gamma_E}{12102274800} + \frac{222333848491\pi^2}{10478160} + \frac{60797852720869631 \log(2)}{4034091600} \right. \\
& \left. - \frac{9604994143653 \log(3)}{531238400} - \frac{120096731201171875 \log(5)}{19916886528} \right) e^4 + \left(-\frac{111072047800937176690152571}{11565838080853056000} \right. \\
& + \frac{236506814452713983\gamma_E}{72613648800} - \frac{32262959758303\pi^2}{62868960} - \frac{16818201812995485953 \log(2)}{72613648800} - \frac{1428503830753023 \log(3)}{16601200} \\
& \left. + \frac{6972609105435390625 \log(5)}{51214851072} + \frac{1673882350937318809 \log(7)}{73164072960} \right) e^6 + \dots + \sigma_{18}e^{18} + \dots \Big]. \tag{5.29}
\end{aligned}$$

The 8PN \log^2 term, meanwhile, was found to have an exact closed-form expression. This form is similar to that of the \mathcal{J}_2 and the \mathcal{J}_{5L} fluxes

$$\begin{aligned}
\mathcal{J}_{8L^2} = & \frac{1}{(1-e^2)^{10}} \left(-\frac{3581369037215}{2178409464} - \frac{80146723840979}{2420454960}e^2 + \frac{1666319275502269}{48409099200}e^4 + \frac{255322553526353183}{290454595200}e^6 \right. \\
& + \frac{49182918759586933}{30981823488}e^8 + \frac{49243901204481373}{61963646976}e^{10} + \frac{634196505488069863}{6196364697600}e^{12} + \frac{47480389267723}{30599331840}e^{14} \Big) \\
& + \frac{40}{(1-e^2)^{17/2}} \left(\frac{366368}{11025} + \frac{37312291}{44100}e^2 + \frac{12067246}{3675}e^4 + \frac{105365147}{35280}e^6 + \frac{42578831}{70560}e^8 + \frac{1614309}{125440}e^{10} \right). \tag{5.30}
\end{aligned}$$

The 8.5PN eccentricity functions were similarly troublesome, yielding coefficients to e^2 , e^{16} , and e^{20} , respectively. We truncated the presentation of the 8.5PN log series at e^6 and leave the remainder of it to [40].

$$\begin{aligned} \mathcal{J}_{17/2} = & \frac{\pi}{(1-e^2)^{21/2}} \left[\frac{60050471374198816098730954501}{1083453442264445091840000} - \frac{16654515688953719\gamma_E}{2020034016000} - \frac{91049249\gamma_E^2}{132300} + \frac{91049249\pi^2}{529200} \right. \\ & - \frac{11256322928659829467 \log(2)}{381786429024000} - \frac{116527141\gamma_E \log(2)}{17150} - \frac{1632801787 \log^2(2)}{185220} - \frac{19606939404628941 \log(3)}{628455027200} \\ & + \frac{5544045\gamma_E \log(3)}{1372} + \frac{5544045 \log(2) \log(3)}{1372} + \frac{5544045 \log^2(3)}{2744} + \frac{49633544921875 \log(5)}{2544182784} - \frac{84807\zeta(3)}{70} \\ & + \left(-\frac{225941369691757950007727558579}{3500388044238976450560000} + \frac{106048473884633692003\gamma_E}{117472747392000} - \frac{276926667149\gamma_E^2}{1852200} + \frac{276926667149\pi^2}{7408800} \right. \\ & - \frac{596136690001068277 \log(2)}{13052527488000} + \frac{307019986547\gamma_E \log(2)}{926100} + \frac{2006541325939 \log^2(2)}{1852200} \\ & + \frac{67576336886522478429 \log(3)}{12569100544000} - \frac{44095962681\gamma_E \log(3)}{68600} - \frac{44095962681 \log(2) \log(3)}{68600} - \frac{44095962681 \log^2(3)}{137200} \\ & \left. - \frac{2935275808466796875 \log(5)}{1163539593216} - \frac{4277552920458643 \log(7)}{10600761600} + \frac{495943519\zeta(3)}{2940} \right) e^2 + \dots \Big], \quad (5.31) \end{aligned}$$

$$\begin{aligned} \mathcal{J}_{17/2L} = & \frac{\pi}{(1-e^2)^{21/2}} \left[\left(-\frac{16654515688953719}{4040068032000} - \frac{91049249\gamma_E}{132300} - \frac{116527141 \log(2)}{34300} + \frac{5544045 \log(3)}{2744} \right) e^2 \right. \\ & + \left(\frac{106048473884633692003}{234945494784000} - \frac{276926667149\gamma_E}{1852200} + \frac{307019986547 \log(2)}{1852200} - \frac{44095962681 \log(3)}{137200} \right) e^4 \\ & + \left(\frac{769384178879100689605873}{73302994372608000} - \frac{132263217227483\gamma_E}{59270400} - \frac{426945632248393 \log(2)}{19756800} + \frac{2672662827537 \log(3)}{627200} \right. \\ & \left. + \frac{5157470703125 \log(5)}{1580544} \right) e^4 + \left(\frac{138182998655659305884296627}{2638907797413888000} - \frac{8915432624231827\gamma_E}{1066867200} \right. \\ & \left. + \frac{309724239257528941 \log(2)}{1066867200} + \frac{4882416222447 \log(3)}{351232} - \frac{12873561103515625 \log(5)}{85349376} \right) e^6 + \dots + \rho_{16} e^{16} + \dots \Big], \quad (5.32) \end{aligned}$$

$$\begin{aligned} \mathcal{J}_{17/2L^2} = & \frac{1}{(1-e^2)^{21/2}} \left(-\frac{91049249}{529200} - \frac{276926667149}{7408800} e^2 - \frac{132263217227483}{237081600} e^4 - \frac{8915432624231827}{4267468800} e^6 \right. \\ & - \frac{138995825711906599}{54623600640} e^8 - \frac{4664651987016654047}{4551966720000} e^{10} - \frac{294210339077129459393}{2621932830720000} e^{12} \\ & - \frac{377078959571059380349}{256949417410560000} e^{14} - \frac{145031943920041772287}{28191021795901440000} e^{16} + \frac{45645187675975688916133}{31968618716552232960000} e^{18} \\ & \left. - \frac{5672267216086086404759471}{25574894973241786368000000} e^{20} + \dots \right). \quad (5.33) \end{aligned}$$

Finally, we find that the 9PN \log^3 term can be expressed in a nice closed form. For further understanding of its origin, see [26].

$$\begin{aligned} \mathcal{J}_{9L^3} = & \frac{1}{(1-e^2)^{11}} \left(\frac{313611008}{3472875} + \frac{44220377171}{6945750} e^2 + \frac{112166162123}{1543500} e^4 + \frac{623241851293}{2646000} e^6 + \frac{1354930634161}{5292000} e^8 \right. \\ & \left. + \frac{52244408821}{564480} e^{10} + \frac{17088124807}{1881600} e^{12} + \frac{96778397}{903168} e^{14} \right). \quad (5.34) \end{aligned}$$

B. Discussion

A careful review of the above results reveals several patterns at the various PN orders, some expected, some rather surprising. Starting at the top, we immediately

notice that the 2PN function \mathcal{J}_2 has a curious form. In Sec. III, we presented a result for this term using the time eccentricity. That function (\mathcal{N}_2) was similar in structure, also being a sum of two finite series with different eccentricity singular factors. However, in the time eccen-

tricity expression, the factors were only separated by a half-power of $(1 - e_t^2)$. In the conversion from time eccentricity to Darwin eccentricity, the subdominant series becomes $(10 - 5/4e^2 - 35/4e^4)$, from which another factor of $(1 - e^2)$ can be removed, leaving a multiple of the Peters term $(1 + 7/8e^2)$.

The more fundamental reason for this behavior remains unknown. However, we have since found that the 2PN energy flux term \mathcal{I}_2 is characterized by a similar simplification. Paper I represented \mathcal{I}_2 with two finite series prefaced by the singular factors $1/(1 - e^2)^{11/2}$ and $1/(1 - e^2)^5$. As we will see in the next section, the subdominant series can be reduced via

$$\begin{aligned} & \frac{1}{(1 - e^2)^5} \left(\frac{35}{2} + \frac{1715}{48}e^2 - \frac{2975}{64}e^4 - \frac{1295}{192}e^6 \right) \\ &= \frac{35}{2(1 - e^2)^4} \left(1 + \frac{73}{24}e^2 + \frac{37}{96}e^4 \right) \end{aligned} \quad (5.35)$$

to obtain a comparable result.

Furthermore, and perhaps most remarkably, analogous forms occur in all found enhancement functions with this dominant-subdominant structure. In both the angular momentum and energy regimes, we note that the $5L$ and $8L^2$ terms contain series from the $3L$ and $6L^2$ terms, respectively.

In total this improved fitting method yielded five new closed-form expressions— \mathcal{J}_{5L} , \mathcal{J}_{6L^2} , \mathcal{J}_{7L^2} , \mathcal{J}_{8L^2} , and \mathcal{J}_{9L^3} . On first glance, it is interesting that such closed representations all involve the first few appearances of a new power of logarithm in the expansion. However, given recent work on logarithmic series [17, 33, 67], this is not surprising. It was this empirical observation that led us to study the origins of these logarithms in the PN expansion more closely, culminating in the characterization of several infinite sets of logarithms in the PN expansion. For instance, the first appearance of each new

power of logarithm is part of a set termed the *leading logarithms*. We have since shown that all leading logarithms can be described by simple Fourier mass quadrupole summations, just like those given in Sec. III C. We refer the reader to [26] for more details.

The 4PN enhancement function is also a case of interest. As with the full flux at 3PN, we see that the transcendentals γ_E and π^2 vanish identically after a certain order in e (here e^8). The specific polynomial prefacing γ_E is proportional to the 4PN log term. Using this fact, one might think it possible to fit our series at 4PN to the form of the full 3PN flux, giving most of the exact series. All that would remain is the 4PN equivalent of $\tilde{\chi}(e)$, which would likely result from the 1PN correction to the tail-of-tails and (tail)² terms that generate $\tilde{\chi}$ at 3PN. This suspicion turns out to be correct, and the relevant details, along with a compact form for \mathcal{J}_4 , will be presented in an upcoming paper [34]. A similar effect occurs in the 6PN Log term, and its compact form was found in [26]. Note that \mathcal{J}_{7L} also shows finite series in γ_E and π^2 . The 5PN function does not, resulting from the fact that \mathcal{J}_{5L} has the aforementioned dominant-subdominant singular factor structure. An exact form for that function will be saved for future investigations.

Moving one step further, we can see a similar simplification in the 6PN integer (non-log) term. The 6PN Log enhancement factor has γ_E and π^2 series that terminate at e^{10} . If we compare the 6PN integer series coefficient of e^{10} to that of e^{12} , we spot a difference: The latter does not contain γ_E^2 , π^4 , or $\gamma_E * \pi^2$. Indeed, these expressions quadratic in the relevant transcendentals vanish, just as their linear counterparts are eliminated in \mathcal{J}_{6L} . The $\zeta(3)$ piece also vanishes at that order, for reasons related to higher order tail integrals [26]. Unfortunately, the dataset was not accurate enough to extract the 7PN integer series beyond e^{12} ; however, we can infer that this series will likely follow a similar pattern, losing all γ_E^2 , π^4 , $\gamma_E * \pi^2$, and $\zeta(3)$ dependence at e^{14} and beyond.

VI. UPDATE: ENERGY FLUX RADIATED TO INFINITY

We now briefly review past work on the energy flux before presenting new results obtained through the procedures developed in this paper. Arun, Blanchet, Iyer, and Qusailah derived 3PN relative-order expansions for the energy flux to infinity for eccentric orbits on Schwarzschild backgrounds in [36] and [37]. Then, in Paper I, we used flux comparisons to find new analytic and numeric e coefficients from 3.5 to 7PN order. Now we work to 8.5PN order (along with the 9PN \log^3 term).

Through 3PN we can preserve the split between instantaneous and hereditary terms:

$$\begin{aligned} \left\langle \frac{dE}{dt} \right\rangle_{\infty} &= \left\langle \frac{dE}{dt} \right\rangle_{\text{N}}^{\infty} \left[\mathcal{I}_0 + y\mathcal{I}_1 + y^{3/2}\mathcal{K}_{3/2} + y^2\mathcal{I}_2 + y^{5/2}\mathcal{K}_{5/2} + y^3(\mathcal{I}_3 + \mathcal{K}_3) + \mathcal{L}_{7/2}y^{7/2} + y^4(\mathcal{L}_4 + \log(y)\mathcal{L}_{4L}) \right. \\ &+ y^{9/2}(\mathcal{L}_{9/2} + \log(y)\mathcal{L}_{9/2L}) + y^5(\mathcal{L}_5 + \log(y)\mathcal{L}_{5L}) + y^{11/2}(\mathcal{L}_{11/2} + \log(y)\mathcal{L}_{11/2L}) \\ &+ y^6(\mathcal{L}_6 + \log(y)\mathcal{L}_{6L} + \log^2(y)\mathcal{L}_{6L^2}) + y^{13/2}(\mathcal{L}_{13/2} + \log(y)\mathcal{L}_{13/2L}) \\ &\left. + y^7(\mathcal{L}_7 + \log(y)\mathcal{L}_{7L} + \log^2(y)\mathcal{L}_{7L^2}) + y^{15/2}(\mathcal{L}_{15/2} + \log(y)\mathcal{L}_{15/2L} + \log^2(y)\mathcal{L}_{15/2L^2}) \right] \end{aligned}$$

$$+ y^8 \left(\mathcal{L}_8 + \log(y) \mathcal{L}_{8L} + \log^2(y) \mathcal{L}_{8L^2} \right) + y^{17/2} \left(\mathcal{L}_{17/2} + \log(y) \mathcal{L}_{17/2L} + \log^2(y) \mathcal{L}_{17/2L^2} \right) + \dots \Big], \quad (6.1)$$

where

$$\left\langle \frac{dE}{dt} \right\rangle_{\text{N}}^{\infty} = \frac{32}{5} \left(\frac{\mu}{M} \right)^2 y^5, \quad (6.2)$$

and

$$\mathcal{I}_0 = \frac{1}{(1-e^2)^{7/2}} \left(1 + \frac{73}{24} e^2 + \frac{37}{96} e^4 \right), \quad (6.3)$$

$$\mathcal{I}_1 = \frac{1}{(1-e^2)^{9/2}} \left(-\frac{1247}{336} - \frac{15901}{672} e^2 - \frac{9253}{384} e^4 - \frac{4037}{1792} e^6 \right), \quad (6.4)$$

$$\mathcal{I}_2 = \frac{1}{(1-e^2)^{11/2}} \left(-\frac{203471}{9072} - \frac{1430873}{18144} e^2 + \frac{2161337}{24192} e^4 + \frac{231899}{2304} e^6 + \frac{499451}{64512} e^8 \right) + \frac{35}{2(1-e^2)^4} \left(1 + \frac{73}{24} e^2 + \frac{37}{96} e^4 \right), \quad (6.5)$$

$$\mathcal{I}_3 = \frac{1}{(1-e^2)^{13/2}} \left[\frac{2193295679}{9979200} + \frac{55022404229}{19958400} e^2 + \frac{68454474929}{13305600} e^4 + \frac{40029894853}{26611200} e^6 - \frac{32487334699}{141926400} e^8 - \frac{233745653}{11354112} e^{10} + \sqrt{1-e^2} \left(-\frac{14047483}{151200} - \frac{75546769}{100800} e^2 - \frac{210234049}{403200} e^4 + \frac{1128608203}{2419200} e^6 + \frac{617515}{10752} e^8 \right) + \frac{1712}{105} \log \left[\frac{y}{y_0} \frac{1 + \sqrt{1-e^2}}{2(1-e^2)} \right] F(e) \right], \quad (6.6)$$

$$\mathcal{K}_{3/2} = \frac{4\pi}{(1-e^2)^5} \left(1 + \frac{1375}{192} e^2 + \frac{3935}{768} e^4 + \frac{10007}{36864} e^6 + \frac{2321}{884736} e^8 - \frac{237857}{353894400} e^{10} + \frac{182863}{4246732800} e^{12} + \frac{4987211}{6658877030400} e^{14} - \frac{47839147}{35514010828800} e^{16} + \dots \right), \quad (6.7)$$

$$\mathcal{K}_{5/2} = \frac{-\pi}{(1-e^2)^6} \left(\frac{8191}{672} + \frac{62003}{336} e^2 + \frac{20327389}{43008} e^4 + \frac{87458089}{387072} e^6 + \frac{67638841}{7077888} e^8 + \frac{332887}{25804800} e^{10} - \frac{482542621}{475634073600} e^{12} + \frac{43302428147}{69918208819200} e^{14} - \frac{2970543742759}{35798122915430400} e^{16} + \dots \right), \quad (6.8)$$

$$\mathcal{K}_3 = -\frac{1712}{105} \chi(e) + \left[-\frac{116761}{3675} + \frac{16}{3} \pi^2 - \frac{1712}{105} \gamma_{\text{E}} - \frac{1712}{105} \log \left(\frac{4y^{3/2}}{y_0} \right) \right] F(e), \quad (6.9)$$

are functions of the Darwin eccentricity e which were known at the time of our previous work (the original functions were given in terms of the time eccentricity, but we quote the converted forms given in Paper I). The \mathcal{I} 's encode instantaneous corrections to the radiated energy, whereas the \mathcal{K} 's are hereditary terms which include effects from the entire orbital history of the particle. Note that like $\tilde{\psi}$, $\mathcal{K}_{5/2}$ has now been extracted to e^{120} .

$F(e)$ and $\chi(e)$ are given by

$$F(e) = \frac{1}{(1-e^2)^{13/2}} \left(1 + \frac{85}{6} e^2 + \frac{5171}{192} e^4 + \frac{1751}{192} e^6 + \frac{297}{1024} e^8 \right), \quad (6.10)$$

and

$$\chi(e) = -\frac{3}{2} F(e) \log(1-e^2) + \frac{1}{(1-e^2)^{13/2}} \left\{ \left[-\frac{3}{2} - \frac{77}{3} \log(2) + \frac{6561}{256} \log(3) \right] e^2 + \left[-22 + \frac{34855}{64} \log(2) - \frac{295245}{1024} \log(3) \right] e^4 + \left[-\frac{6595}{128} - \frac{1167467}{192} \log(2) + \frac{24247269}{16384} \log(3) + \frac{244140625}{147456} \log(5) \right] e^6 \right\} \quad (6.11)$$

$$+ \left[-\frac{31747}{768} + \frac{122348557}{3072} \log(2) + \frac{486841509}{131072} \log(3) - \frac{23193359375}{1179648} \log(5) \right] e^8 + \dots \Big\}.$$

Now we move beyond 3PN order. Like the \mathcal{J}_i of the previous section, these $\mathcal{L}_i(e)$ functions are calculated using lmn fitting. Coefficients are given to 8.5PN order in y and varying orders in eccentricity as needed (full results will be posted to the BHP Toolkit). Here, the use of a Roman letter (e.g. b_{30}) denotes the highest power for which we retrieved an analytic form. As with the angular momentum, we are not able to distinguish between instantaneous and hereditary terms at this level, so the \mathcal{L} 's generically include both contributions. A subset of these coefficients were first produced in Paper I.

$$\begin{aligned} \mathcal{L}_{7/2} = & \frac{\pi}{(1-e^2)^7} \left(-\frac{16285}{504} - \frac{21500207}{48384} e^2 - \frac{3345329}{48384} e^4 + \frac{111594754909}{41803776} e^6 + \frac{82936785623}{55738368} e^8 + \frac{11764982139179}{107017666560} e^{10} \right. \\ & + \frac{216868426237103}{9631589990400} e^{12} + \frac{30182578123501193}{2517055517491200} e^{14} + \frac{351410391437739607}{48327465935831040} e^{16} + \frac{1006563319333377521717}{208774652842790092800} e^{18} \\ & + \frac{138433556497603036591}{40776299383357440000} e^{20} + \frac{16836217054749609972406421}{6736462131727360327680000} e^{22} + \frac{2077866815397007172515220959}{1091306865339832373084160000} e^{24} \\ & + \frac{6702459208696786891810972264771}{4496600021148810265629818880000} e^{26} + \frac{1003693903183075635039911792668567}{841272985774931956969651568640000} e^{28} \\ & \left. + \frac{2160389373606905789762084388554056897}{2220960682445820366399880141209600000} e^{30} + \dots \right), \quad (6.12) \end{aligned}$$

$$\begin{aligned} \mathcal{L}_4 = & \frac{1}{(1-e^2)^{15/2}} \left[\frac{323105549467}{3178375200} + \frac{232597\gamma_E}{4410} - \frac{1369\pi^2}{126} + \frac{39931 \log(2)}{294} - \frac{47385 \log(3)}{1568} + \left(-\frac{128412398137}{23543520} \right. \right. \\ & + \frac{4923511\gamma_E}{2940} - \frac{104549\pi^2}{252} - \frac{343177 \log(2)}{252} + \frac{55105839 \log(3)}{15680} \Big) e^2 + \left(-\frac{981480754818517}{25427001600} + \frac{142278179\gamma_E}{17640} \right. \\ & - \frac{1113487\pi^2}{504} + \frac{762077713 \log(2)}{5880} - \frac{2595297591 \log(3)}{71680} - \frac{15869140625 \log(5)}{903168} \Big) e^4 + \left(-\frac{874590390287699}{12713500800} \right. \\ & + \frac{318425291\gamma_E}{35280} - \frac{881501\pi^2}{336} - \frac{90762985321 \log(2)}{63504} + \frac{31649037093 \log(3)}{1003520} + \frac{10089048828125 \log(5)}{16257024} \Big) e^6 \\ & + \left(-\frac{588262620227803}{15647385600} + \frac{1256401651\gamma_E}{564480} - \frac{3609941\pi^2}{5376} + \frac{60196618062379 \log(2)}{5080320} + \frac{103481536492359 \log(3)}{25690112} \right. \\ & - \frac{13689354185546875 \log(5)}{2080899072} - \frac{44084499735185 \log(7)}{42467328} \Big) e^8 + \left(-\frac{2506068425640457}{271221350400} + \frac{7220691\gamma_E}{125440} - \frac{63771\pi^2}{3584} \right. \\ & - \frac{7802806392729223 \log(2)}{84672000} - \frac{304325022941627589 \log(3)}{6422528000} + \frac{52671902802734375 \log(5)}{1387266048} \\ & + \frac{99735805288105217 \log(7)}{3538944000} \Big) e^{10} + \left(-\frac{205790655085493}{33210777600} + \frac{9036104785041317 \log(2)}{11430720} \right. \\ & + \frac{4775869078725402009 \log(3)}{20552089600} - \frac{4795866464849609375 \log(5)}{33294385152} - \frac{179568613346696178017 \log(7)}{611529523200} \Big) e^{12} + \dots \\ & \left. + a_{30} e^{30} + \dots \right], \quad (6.13) \end{aligned}$$

$$\mathcal{L}_{4L} = \frac{1}{(1-e^2)^{15/2}} \left(\frac{232597}{8820} + \frac{4923511}{5880} e^2 + \frac{142278179}{35280} e^4 + \frac{318425291}{70560} e^6 + \frac{1256401651}{1128960} e^8 + \frac{7220691}{250880} e^{10} \right), \quad (6.14)$$

$$\begin{aligned} \mathcal{L}_{9/2} = & \frac{\pi}{(1-e^2)^8} \left(\frac{265978667519}{745113600} - \frac{6848\gamma_E}{105} - \frac{13696 \log(2)}{105} + \left(\frac{5031659060513}{447068160} - \frac{418477\gamma_E}{252} - \frac{1024097 \log(2)}{1260} \right. \right. \\ & - \frac{702027 \log(3)}{280} \Big) e^2 + \left(\frac{4137488075571679}{71530905600} - \frac{32490229\gamma_E}{5040} - \frac{56349731 \log(2)}{720} + \frac{35803377 \log(3)}{1120} \right) e^4 \\ & + \left(\frac{119161057323769}{1609445376} - \frac{283848209\gamma_E}{48384} + \frac{212985174443 \log(2)}{241920} - \frac{481356513 \log(3)}{2560} - \frac{26123046875 \log(5)}{96768} \right) e^6 \\ & + \left(\frac{916628147773341301}{65922882600960} - \frac{1378010735\gamma_E}{1161216} - \frac{8023715124847 \log(2)}{1161216} - \frac{135922489587 \log(3)}{143360} \right) e^8 \end{aligned}$$

$$+ \frac{2795166015625 \log(5)}{774144} \Big) e^8 + \dots + b_{30} b^{30} + \dots \Big], \quad (6.15)$$

$$\begin{aligned} \mathcal{L}_{9/2L} = & \frac{\pi}{(1-e^2)^8} \left(-\frac{3424}{105} - \frac{418477}{504} e^2 - \frac{32490229}{10080} e^4 - \frac{283848209}{96768} e^6 - \frac{1378010735}{2322432} e^8 - \frac{59600244089}{4644864000} e^{10} \right. \\ & + \frac{482765917}{7962624000} e^{12} - \frac{532101153539}{29132587008000} e^{14} + \frac{576726373021}{199766310912000} e^{16} - \frac{98932878601597}{3624559945187328000} e^{18} \\ & - \frac{56946683948951263}{1087367983556198400000} e^{20} - \frac{90233805781037113}{60146983318994288640000} e^{22} + \frac{73049155670984045033}{50523465987955202457600000} e^{24} \\ & + \frac{30834120217438664094539}{81969271218858520467210240000} e^{26} + \frac{4892777190662608136893709}{80329885794481350057866035200000} e^{28} \\ & \left. + \frac{625894086470885360433206659}{77116690362702096055551393792000000} e^{30} + \dots \right), \quad (6.16) \end{aligned}$$

$$\begin{aligned} \mathcal{L}_5 = & \frac{1}{(1-e^2)^{17/2}} \left[-\frac{2500861660823683}{2831932303200} + \frac{916628467\gamma_E}{7858620} - \frac{424223\pi^2}{6804} - \frac{83217611 \log(2)}{1122660} + \frac{47385 \log(3)}{196} \right. \\ & + \left(-\frac{121566202635820681}{5663864606400} + \frac{11627266729\gamma_E}{15717240} - \frac{16845407\pi^2}{13608} + \frac{41528347547 \log(2)}{1428840} \right. \\ & - \frac{1380946887 \log(3)}{137984} - \frac{383544921875 \log(5)}{100590336} \Big) e^2 + \left(-\frac{886493383307889029}{15103638950400} - \frac{84010607399\gamma_E}{5239080} \right. \\ & - \frac{14848651\pi^2}{9072} - \frac{3992455076567 \log(2)}{5239080} + \frac{61777429029 \log(3)}{2759680} + \frac{120783447265625 \log(5)}{402361344} \Big) e^4 \\ & + \left(\frac{11463059954793067}{53495769600} - \frac{67781855563\gamma_E}{816480} + \frac{111910879\pi^2}{7776} + \frac{1925006801181043 \log(2)}{188606880} \right. \\ & \left. \left. + \frac{153356656665033 \log(3)}{44154880} - \frac{30664709673671875 \log(5)}{5267275776} - \frac{1065488447445779 \log(7)}{1182449664} \right) e^6 + \dots + c_{30} e^{30} + \dots \right], \quad (6.17) \end{aligned}$$

$$\begin{aligned} \mathcal{L}_{5L} = & \frac{1}{(1-e^2)^{17/2}} \left(\frac{5080948627}{15717240} + \frac{117123377449}{31434480} e^2 - \frac{4199642054}{654885} e^4 - \frac{78989239933}{1632960} e^6 - \frac{88593702010771}{2011806720} e^8 \right. \\ & \left. - \frac{261925436695}{29804544} e^{10} - \frac{245975507}{1290240} e^{12} \right) - \frac{65}{2(1-e^2)^7} \left(\frac{856}{105} + \frac{7276}{63} e^2 + \frac{553297}{2520} e^4 + \frac{187357}{2520} e^6 + \frac{10593}{4480} e^8 \right), \quad (6.18) \end{aligned}$$

$$\begin{aligned} \mathcal{L}_{11/2} = & \frac{\pi}{(1-e^2)^9} \left[\frac{8399309750401}{101708006400} + \frac{177293\gamma_E}{1176} + \frac{8521283 \log(2)}{17640} - \frac{142155 \log(3)}{784} + \left(-\frac{6454125584294467}{203416012800} \right. \right. \\ & + \frac{197515529\gamma_E}{17640} - \frac{195924727 \log(2)}{17640} + \frac{1909251 \log(3)}{80} \Big) e^2 + \left(-\frac{354252739653461867}{813664051200} + \frac{22177125281\gamma_E}{225792} \right. \\ & + \frac{1349842104869 \log(2)}{1128960} - \frac{14094701055 \log(3)}{50176} - \frac{79345703125 \log(5)}{451584} \Big) e^4 + \left(-\frac{3220604701659665695}{2343352467456} \right. \\ & + \frac{362637121649\gamma_E}{1693440} - \frac{551674667051 \log(2)}{37632} - \frac{28712823381 \log(3)}{125440} + \frac{14134345703125 \log(5)}{2032128} \Big) e^6 \\ & \left. + \dots + d_{30} e^{30} + \dots \right], \quad (6.19) \end{aligned}$$

$$\begin{aligned} \mathcal{L}_{11/2L} = & \frac{\pi}{(1-e^2)^9} \left(\frac{177293}{2352} + \frac{197515529}{35280} e^2 + \frac{22177125281}{451584} e^4 + \frac{362637121649}{3386880} e^6 + \frac{175129893794507}{2601123840} e^8 \right. \\ & + \frac{137611940506079}{13005619200} e^{10} + \frac{75058973874797}{396361728000} e^{12} + \frac{1045783525483}{131096641536000} e^{14} + \frac{44925442631482501}{1879401453060096000} e^{16} \\ & - \frac{801339891963050743}{50743839232622592000} e^{18} + \frac{719061383331468255529}{243570428316588441600000} e^{20} + \frac{14491034377225531751}{421028883232960020480000} e^{22} \\ & - \frac{48380310946786430680357}{1028841489209269577318400000} e^{24} + \frac{328896042939144986202607}{117098958884083600667443200000} e^{26} \\ & \left. + \frac{12426147326832099974747530661}{5536582897835022280911382118400000} e^{28} + \frac{1156253390804057519850290651}{5623092005613694504050622464000000} e^{30} + \dots \right), \quad (6.20) \end{aligned}$$

$$\begin{aligned}
\mathcal{L}_6 = & \frac{1}{(1-e^2)^{19/2}} \left[\frac{2067586193789233570693}{602387400044430000} - \frac{246137536815857\gamma_E}{157329572400} + \frac{1465472\gamma_E^2}{11025} + \frac{3803225263\pi^2}{10478160} - \frac{27392\gamma_E\pi^2}{315} \right. \\
& - \frac{256\pi^4}{45} - \frac{271272899815409 \log(2)}{157329572400} + \frac{5861888\gamma_E \log(2)}{11025} - \frac{54784}{315}\pi^2 \log(2) + \frac{5861888 \log^2(2)}{11025} \\
& - \frac{437114506833 \log(3)}{789268480} - \frac{37744140625 \log(5)}{260941824} - \frac{27392\zeta(3)}{105} + \left(\frac{620642724143587842589757}{2409549600177720000} \right. \\
& - \frac{25915820507512391\gamma_E}{314659144800} + \frac{189812971\gamma_E^2}{33075} + \frac{8630456095\pi^2}{381024} - \frac{3547906\gamma_E\pi^2}{945} - \frac{33158\pi^4}{135} \\
& - \frac{1204827593616887 \log(2)}{6421615200} + \frac{36018554\gamma_E \log(2)}{4725} - \frac{336622}{135}\pi^2 \log(2) - \frac{57245 \log^2(2)}{1323} - \frac{425707669538577 \log(3)}{4249907200} \\
& + \frac{75116889\gamma_E \log(3)}{4900} - \frac{702027}{140}\pi^2 \log(3) + \frac{75116889 \log(2) \log(3)}{4900} + \frac{75116889 \log^2(3)}{9800} \\
& + \frac{1735378662109375 \log(5)}{32878669824} - \frac{3547906\zeta(3)}{315} \Big) e^2 + \left(\frac{866764151375288467902617}{321273280023696000} - \frac{56861331626354501\gamma_E}{83909105280} \right. \\
& + \frac{1052380631\gamma_E^2}{26460} + \frac{106659145841\pi^2}{508032} - \frac{9835333\gamma_E\pi^2}{378} - \frac{91919\pi^4}{54} - \frac{469561807262423641 \log(2)}{419545526400} \\
& + \frac{42983885171\gamma_E \log(2)}{66150} - \frac{401718553\pi^2 \log(2)}{1890} + \frac{6177731563 \log^2(2)}{5292} + \frac{4967869967044739217 \log(3)}{1767961395200} \\
& - \frac{4281662673\gamma_E \log(3)}{19600} + \frac{40015539}{560}\pi^2 \log(3) - \frac{4281662673 \log(2) \log(3)}{19600} - \frac{4281662673 \log^2(3)}{39200} \\
& - \frac{1749708882763671875 \log(5)}{818313560064} - \frac{25689055330301573 \log(7)}{83501383680} - \frac{9835333\zeta(3)}{126} \Big) e^4 + \dots \\
& + \left(\frac{24612086555137636537042301}{131593535497705881600} - \frac{477961162088755717\gamma_E}{7160243650560} + \frac{32323997924497\pi^2}{1430618112} \right. \\
& - \frac{61278163606788680414049737704313 \log(2)}{31971382930206720000} - \frac{339392544622900323521\gamma_E \log(2)}{8751645000} \\
& + \frac{3171892940400937603\pi^2 \log(2)}{250047000} - \frac{4532425889525064665801 \log^2(2)}{52509870000} - \frac{15568492847979888930357\gamma_E \log(3)}{3147038720000} \\
& + \frac{9519685411620604508156942363799 \log(3)}{8870923096555520000} - \frac{46776237102385425837621 \log(2) \log(3)}{3147038720000} \\
& + \frac{145499933158690550751\pi^2 \log(3)}{89915392000} - \frac{25647883085450625849 \log^2(3)}{1573519360000} + \frac{20971917520162841796875\gamma_E \log(5)}{5506058944512} \\
& - \frac{2425918968367925016852218629596875 \log(5)}{6704884965484888326144} + \frac{20971917520162841796875 \log(2) \log(5)}{5506058944512} \\
& - \frac{979996145802001953125\pi^2 \log(5)}{786579849216} + \frac{20971917520162841796875 \log^2(5)}{11012117889024} + \frac{77148041218710802588787\gamma_E \log(7)}{5733089280000} \\
& + \frac{11539161795601951836966750333833 \log(7)}{49866759129268224000} - \frac{5047068117111921664687\pi^2 \log(7)}{1146617856000} \\
& + \frac{77148041218710802588787 \log(2) \log(7)}{5733089280000} + \frac{77148041218710802588787 \log^2(7)}{11466178560000} \\
& \left. + \frac{8938746466657465062086011285151 \log(11)}{76115758848933888000} \right) e^{14} + \dots + f_{20}e^{20} + \dots \Big], \tag{6.21}
\end{aligned}$$

$$\begin{aligned}
\mathcal{L}_{6L} = & \frac{1}{(1-e^2)^{19/2}} \left[-\frac{246137536815857}{314659144800} + \frac{1465472\gamma_E}{11025} - \frac{13696\pi^2}{315} + \frac{2930944 \log(2)}{11025} + \left(-\frac{25915820507512391}{629318289600} \right. \right. \\
& + \frac{189812971\gamma_E}{33075} - \frac{1773953\pi^2}{945} + \frac{18009277 \log(2)}{4725} + \frac{75116889 \log(3)}{9800} \Big) e^2 + \left(-\frac{56861331626354501}{167818210560} \right. \\
& + \frac{1052380631\gamma_E}{26460} - \frac{9835333\pi^2}{756} + \frac{42983885171 \log(2)}{132300} - \frac{4281662673 \log(3)}{39200} \Big) e^4 + \left(-\frac{710806279550045831}{1006909263360} \right. \\
& \left. + \frac{9707068997\gamma_E}{132300} - \frac{90720271\pi^2}{3780} - \frac{519508209691 \log(2)}{132300} + \frac{454281905709 \log(3)}{627200} + \frac{2795166015625 \log(5)}{2032128} \right) e^6
\end{aligned}$$

$$\begin{aligned}
& + \left(-\frac{10213351238593603069}{40276370534400} + \frac{8409851501\gamma_E}{211680} - \frac{78596743\pi^2}{6048} + \frac{117139032193219 \log(2)}{3175200} \right. \\
& + \frac{6991554521601 \log(3)}{1003520} - \frac{47517822265625 \log(5)}{2322432} \left. \right) e^8 + \left(\frac{3985515397336843519}{26850913689600} + \frac{4574665481\gamma_E}{846720} \right. \\
& - \frac{42753883\pi^2}{24192} - \frac{252510878807655859 \log(2)}{952560000} - \frac{576360297584196039 \log(3)}{4014080000} + \frac{223101765869140625 \log(5)}{1560674304} \\
& + \frac{380483822091361849 \log(7)}{6635520000} \left. \right) e^{10} + \left(\frac{50719954422267749}{3254656204800} + \frac{6308399\gamma_E}{75264} - \frac{294785\pi^2}{10752} \right. \\
& + \frac{2887481794238961637 \log(2)}{1270080000} + \frac{17322463230547056201 \log(3)}{16056320000} - \frac{1297619485595703125 \log(5)}{2080899072} \\
& - \frac{2663386754639532943 \log(7)}{2949120000} \left. \right) e^{12} + \left(-\frac{477961162088755717}{14320487301120} - \frac{339392544622900323521 \log(2)}{17503290000} \right. \\
& - \frac{15568492847979888930357 \log(3)}{6294077440000} + \frac{20971917520162841796875 \log(5)}{11012117889024} \\
& + \left. \frac{77148041218710802588787 \log(7)}{11466178560000} \right) e^{14} + \dots + g_{30}e^{30} + \dots \Big], \tag{6.22}
\end{aligned}$$

$$\begin{aligned}
\mathcal{L}_{6L^2} = \frac{1}{(1-e^2)^{19/2}} & \left(\frac{366368}{11025} + \frac{189812971}{132300} e^2 + \frac{1052380631}{105840} e^4 + \frac{9707068997}{529200} e^6 \right. \\
& \left. + \frac{8409851501}{846720} e^8 + \frac{4574665481}{3386880} e^{10} + \frac{6308399}{301056} e^{12} \right), \tag{6.23}
\end{aligned}$$

$$\begin{aligned}
\mathcal{L}_{13/2} = \frac{\pi}{(1-e^2)^{10}} & \left[-\frac{81605095538444363}{20138185267200} + \frac{300277177\gamma_E}{436590} - \frac{42817273 \log(2)}{71442} + \frac{142155 \log(3)}{98} \right. \\
& + \left(-\frac{486006274042153993}{3098182348800} + \frac{99375022631\gamma_E}{13970880} + \frac{30885453339487 \log(2)}{125737920} - \frac{26221716657 \log(3)}{344960} \right. \\
& - \frac{1917724609375 \log(5)}{50295168} \left. \right) e^2 + \left(-\frac{978074410273210177483}{1288843857100800} - \frac{206420323339\gamma_E}{1164240} - \frac{35044764797711 \log(2)}{4490640} \right. \\
& - \frac{896501601 \log(3)}{12320} + \frac{82230224609375 \log(5)}{25147584} \left. \right) e^4 + \left(\frac{1759614571265146017649}{652477202657280} - \frac{52528099035138203\gamma_E}{36212520960} \right. \\
& + \frac{490814480869706621 \log(2)}{4023613440} + \frac{1040915745740691 \log(3)}{22077440} - \frac{2078689555036328125 \log(5)}{28970016768} \\
& \left. - \frac{7458419132120453 \log(7)}{591224832} \right) e^6 + \dots + h_{28}e^{28} + \dots \Big], \tag{6.24}
\end{aligned}$$

$$\begin{aligned}
\mathcal{L}_{13/2L} = \frac{\pi}{(1-e^2)^{10}} & \left(\frac{300277177}{873180} + \frac{99375022631}{27941760} e^2 - \frac{206420323339}{2328480} e^4 - \frac{52528099035138203}{72425041920} e^6 \right. \\
& - \frac{133623698374169077}{96566722560} e^8 - \frac{13064004066588147059}{16855282483200} e^{10} - \frac{1963639930072973146717}{16686729658368000} e^{12} \\
& - \frac{33400949279751680423063}{4360798684053504000} e^{14} - \frac{179371445578657546009993}{59805239095590912000} e^{16} - \frac{637047737965052868548277511}{361702086050133835776000} e^{18} \\
& - \frac{3460275187517318400615660587}{3014184050417781964800000} e^{20} - \frac{27996584084597317460228073711577}{35012761929652955303116800000} e^{22} \\
& - \frac{19726180767340366267420639753777}{33762306146451064042291200000} e^{24} - \frac{24140999291524879880417880052762466303}{54532516756482196496425628467200000} e^{26} - \\
& \left. \frac{5533246861404900450857176595606015862331}{16032559926405765769949134769356800000} e^{28} - \frac{39240045588213441329120436124666666397117}{142511643790273473510658975727616000000} e^{30} + \dots \right), \tag{6.25}
\end{aligned}$$

$$\begin{aligned}
\mathcal{L}_7 = \frac{1}{(1-e^2)^{21/2}} & \left[\frac{58327313257446476199371189}{8332222517414555760000} + \frac{9640384387033067\gamma_E}{17896238860500} - \frac{52525903\gamma_E^2}{154350} + \frac{2621359845833\pi^2}{2383781400} \right. \\
& + \frac{531077\gamma_E\pi^2}{6615} - \frac{9523\pi^4}{945} + \frac{19402232550751339 \log(2)}{17896238860500} - \frac{471188717\gamma_E \log(2)}{231525} + \frac{128223}{245} \pi^2 \log(2) \left. \right]
\end{aligned}$$

$$\begin{aligned}
& - \frac{5811697 \log^2(2)}{2450} - \frac{6136997968378863 \log(3)}{1256910054400} + \frac{1848015 \gamma_E \log(3)}{2744} - \frac{142155}{392} \pi^2 \log(3) + \frac{1848015 \log(2) \log(3)}{2744} \\
& + \frac{1848015 \log^2(3)}{5488} + \frac{9926708984375 \log(5)}{5088365568} + \frac{531077 \zeta(3)}{2205} + \left(- \frac{1833694744307038499536301503}{3332889006965822304000} \right. \\
& + \frac{5361621824744487121 \gamma_E}{14316991088400} - \frac{8436767071 \gamma_E^2}{185220} - \frac{131503074649 \pi^2}{3531528} + \frac{20170061 \gamma_E \pi^2}{882} + \frac{283391 \pi^4}{378} \\
& + \frac{2977365445451226901 \log(2)}{71584955442000} + \frac{8661528101 \gamma_E \log(2)}{463050} - \frac{440469373 \pi^2 \log(2)}{13230} + \frac{154654591013 \log^2(2)}{926100} \\
& + \frac{12486523458893227371 \log(3)}{12569100544000} - \frac{21008472903 \gamma_E \log(3)}{137200} + \frac{208895679 \pi^2 \log(3)}{3920} - \frac{21008472903 \log(2) \log(3)}{137200} \\
& - \frac{21008472903 \log^2(3)}{274400} - \frac{80233643837890625 \log(5)}{268509136896} - \frac{4277552920458643 \log(7)}{127209139200} + \frac{20170061 \zeta(3)}{294} \Big) e^2 \\
& + \left(- \frac{425327739088776761686492357}{27207257199720998400} + \frac{69100209694441952051 \gamma_E}{10226422206000} - \frac{66537493061 \gamma_E^2}{105840} - \frac{3452732996641507 \pi^2}{2724321600} \right. \\
& + \frac{530883301 \gamma_E \pi^2}{1512} + \frac{17810521 \pi^4}{1080} + \frac{565134631654755855073 \log(2)}{14316991088400} - \frac{18504183154799 \gamma_E \log(2)}{1852200} \\
& + \frac{63724032709 \pi^2 \log(2)}{17640} - \frac{13381694922467 \log^2(2)}{740880} - \frac{9013628727200023913673 \log(3)}{402211217408000} \\
& + \frac{1804462952967 \gamma_E \log(3)}{878080} - \frac{17687032263 \pi^2 \log(3)}{25088} + \frac{1804462952967 \log(2) \log(3)}{878080} + \frac{1804462952967 \log^2(3)}{1756160} \\
& - \frac{722647442175224609375 \log(5)}{2345695819923456} + \frac{5157470703125 \gamma_E \log(5)}{4741632} - \frac{396728515625 \pi^2 \log(5)}{677376} \\
& + \frac{5157470703125 \log(2) \log(5)}{4741632} + \frac{5157470703125 \log^2(5)}{9483264} + \frac{130895018390638453 \log(7)}{20102184960} + \frac{530883301 \zeta(3)}{504} \Big) e^4 \\
& + \dots + j_{12} e^{12} + \dots \Big], \tag{6.26}
\end{aligned}$$

$$\begin{aligned}
\mathcal{L}_{7L} = & \frac{1}{(1-e^2)^{21/2}} \left[\frac{9640384387033067}{35792477721000} - \frac{52525903 \gamma_E}{154350} + \frac{531077 \pi^2}{13230} - \frac{471188717 \log(2)}{463050} + \frac{1848015 \log(3)}{5488} \right. \\
& + \left(\frac{5361621824744487121}{28633982176800} - \frac{8436767071 \gamma_E}{185220} + \frac{20170061 \pi^2}{1764} + \frac{8661528101 \log(2)}{926100} - \frac{21008472903 \log(3)}{274400} \right) e^2 \\
& + \left(\frac{69100209694441952051}{20452844412000} - \frac{66537493061 \gamma_E}{105840} + \frac{530883301 \pi^2}{3024} - \frac{18504183154799 \log(2)}{3704400} \right. \\
& + \frac{1804462952967 \log(3)}{1756160} + \frac{5157470703125 \log(5)}{9483264} \Big) e^4 + \dots + \left(\frac{392956261308991697579}{222130285977600} - \frac{6441767405 \gamma_E}{4214784} \right. \\
& + \frac{290022625 \pi^2}{602112} + \frac{79758263769894173174170363 \log(2)}{94097687040000} - \frac{4735538949816648321845247 \log(3)}{176234168320000} \\
& - \frac{11353999155433772705078125 \log(5)}{308339300892672} - \frac{87075197521422359501707 \log(7)}{339738624000} \Big) e^{14} + \left(\frac{14816695856807173325147}{9477558868377600} \right. \\
& - \frac{5064686588825332952885407 \log(2)}{840157920000} + \frac{42721403084890740280304298693 \log(3)}{22557973544960000} \\
& - \frac{205760911201132587653505859375 \log(5)}{631478888228192256} + \frac{29799003038979039956177798137 \log(7)}{23482733690880000} \\
& \left. + \frac{201417183487589839275762436609 \log(11)}{3157394441140961280} \right) e^{16} + \dots + k_{26} e^{26} + \dots \Big], \tag{6.27}
\end{aligned}$$

$$\begin{aligned}
\mathcal{L}_{7L^2} = & - \frac{1}{(1-e^2)^{21/2}} \left(\frac{52525903}{617400} + \frac{8436767071}{740880} e^2 + \frac{66537493061}{423360} e^4 + \frac{16839575984743}{29635200} e^6 + \frac{22951910431067}{33868800} e^8 \right. \\
& \left. + \frac{18225509849041}{67737600} e^{10} + \frac{2633534008997}{90316800} e^{12} + \frac{6441767405}{16859136} e^{14} \right), \tag{6.28}
\end{aligned}$$

$$\begin{aligned}
\mathcal{L}_{15/2} = & \frac{1}{(1-e^2)^{11}} \left[\frac{51603801120086143145449}{8567287467298560000} - \frac{3025414963439009\gamma_E}{559394035200} + \frac{5861888\gamma_E^2}{11025} - \frac{1465472\pi^2}{11025} \right. \\
& - \frac{1999998476702377 \log(2)}{5034546316800} + \frac{23447552\gamma_E \log(2)}{11025} + \frac{23447552 \log^2(2)}{11025} - \frac{1311343520499 \log(3)}{394634240} \\
& - \frac{188720703125 \log(5)}{130470912} - \frac{109568\zeta(3)}{105} + \left(\frac{617542475472651187592698603}{411229798430330880000} - \frac{439734196881760549\gamma_E}{839091052800} \right. \\
& + \frac{2479658767\gamma_E^2}{66150} - \frac{2479658767\pi^2}{264600} - \frac{106026671002494841 \log(2)}{64545465600} + \frac{1916917519\gamma_E \log(2)}{33075} + \frac{791435023 \log^2(2)}{66150} \\
& - \frac{4420920979736127 \log(3)}{6906099200} + \frac{225350667\gamma_E \log(3)}{2450} + \frac{225350667 \log(2) \log(3)}{2450} + \frac{225350667 \log^2(3)}{4900} \\
& + \frac{15905145751953125 \log(5)}{28768836096} - \frac{23174381\zeta(3)}{315} \Big) e^2 + \left(\frac{1484918820873890610249964661}{54830639790710784000} \right. \\
& - \frac{126350957261075251487\gamma_E}{17900609126400} + \frac{22643958139\gamma_E^2}{52920} - \frac{22643958139\pi^2}{211680} + \frac{133444424175863332003 \log(2)}{53701827379200} \\
& + \frac{706231828327\gamma_E \log(2)}{132300} + \frac{2468502941543 \log^2(2)}{264600} + \frac{62442239264166123 \log(3)}{2296053760} - \frac{2028156003\gamma_E \log(3)}{1400} \\
& - \frac{2028156003 \log(2) \log(3)}{1400} - \frac{2028156003 \log^2(3)}{2800} - \frac{2354821775634765625 \log(5)}{94420795392} - \frac{179823387312111011 \log(7)}{41750691840} \\
& \left. - \frac{211625777\zeta(3)}{252} \right) e^4 + \dots + l_{12}e^{12} + \dots, \tag{6.29}
\end{aligned}$$

$$\begin{aligned}
\mathcal{L}_{15/2L} = & \frac{1}{(1-e^2)^{11}} \left[-\frac{3025414963439009}{1118788070400} + \frac{5861888\gamma_E}{11025} + \frac{11723776 \log(2)}{11025} + \left(-\frac{439734196881760549}{1678182105600} \right. \right. \\
& + \frac{2479658767\gamma_E}{66150} + \frac{1916917519 \log(2)}{66150} + \frac{225350667 \log(3)}{4900} \Big) e^2 + \left(-\frac{126350957261075251487}{35801218252800} \right. \\
& + \frac{22643958139\gamma_E}{52920} + \frac{706231828327 \log(2)}{264600} - \frac{2028156003 \log(3)}{2800} \Big) e^4 + \left(-\frac{36144975344017995555691}{2899898678476800} \right. \\
& + \frac{17616792537263\gamma_E}{12700800} - \frac{428644895504209 \log(2)}{12700800} + \frac{1676533845591 \log(3)}{313600} + \frac{13975830078125 \log(5)}{1016064} \Big) e^6 \\
& + \left(-\frac{1465091734136920643784967}{134977102125465600} + \frac{459691434479657\gamma_E}{304819200} + \frac{23409352359075029 \log(2)}{60963840} \right. \\
& \left. + \frac{237441706804107 \log(3)}{2508800} - \frac{1830833740234375 \log(5)}{8128512} \right) e^8 + \dots + m_{26}e^{26} + \dots, \tag{6.30}
\end{aligned}$$

$$\begin{aligned}
\mathcal{L}_{15/2L^2} = & \frac{1}{(1-e^2)^{11}} \left(\frac{1465472}{11025} + \frac{2479658767}{264600} e^2 + \frac{22643958139}{211680} e^4 + \frac{17616792537263}{50803200} e^6 + \frac{459691434479657}{1219276800} e^8 \right. \\
& + \frac{66494784224478367}{487710720000} e^{10} + \frac{78360178393945783}{5852528640000} e^{12} + \frac{1444655514143830483}{9176764907520000} e^{14} + \frac{51015640024026887}{146828238520320000} e^{16} \\
& - \frac{43873302622896741181}{380578794244669440000} e^{18} + \frac{373288343491048076867}{16310519753342976000000} e^{20} - \frac{286026594234455117352479}{221040163697304010752000000} e^{22} \\
& - \frac{2464347696391370853689}{6062815918554624294912000} e^{24} + \frac{1224305061272403640352089951}{43033867389900723245285376000000} e^{26} \\
& \left. + \frac{120162136825359369885614962913}{8434638008420541756075933696000000} e^{28} + \dots \right), \tag{6.31}
\end{aligned}$$

$$\begin{aligned}
\mathcal{L}_8 \approx & \frac{1}{(1-e^2)^{21/2}} \left(-\frac{2206020140875740874945597498877}{63104087235639138048360000} + \frac{17328950668070007334987\gamma_E}{1084297320079974000} - \frac{3428849385499\gamma_E^2}{2723011830} \right. \\
& - \frac{18584197930153871\pi^2}{4247898454800} + \frac{1397063663\gamma_E\pi^2}{1178793} + \frac{2192471\pi^4}{25515} - \frac{4773986555637567504053 \log(2)}{1084297320079974000} \\
& + \frac{15332591650681\gamma_E \log(2)}{6807529575} - \frac{11366135381}{5893965} \pi^2 \log(2) + \frac{106165554403193 \log^2(2)}{13615059150} + \frac{8479423463263174971 \log(3)}{213674709248000} \\
& - \frac{1848015\gamma_E \log(3)}{343} + \frac{142155}{49} \pi^2 \log(3) - \frac{1848015 \log(2) \log(3)}{343} - \frac{1848015 \log^2(3)}{686} - \frac{83415474560546875 \log(5)}{8477217036288}
\end{aligned}$$

$$\begin{aligned}
& - \frac{2025852318599963 \log(7)}{2948939136000} + \frac{1397063663\zeta(3)}{392931} - 3445110.45223167809957813155e^2 - \\
& 63011640.2589502111479578408e^4 - 273933223.6521104390237430479e^6 - 325300545.71499163564006669284e^8 + \\
& 77909913.97444552477119497207e^{10}), \tag{6.32}
\end{aligned}$$

$$\begin{aligned}
\mathcal{L}_{8L} = & \frac{1}{(1-e^2)^{23/2}} \left[\frac{17254929304352547776587}{2168594640159948000} - \frac{3428849385499\gamma_E}{2723011830} + \frac{1397063663\pi^2}{2357586} + \frac{15332591650681 \log(2)}{13615059150} \right. \\
& - \frac{1848015 \log(3)}{686} + \left(\frac{131085309923714183816419}{619598468617128000} + \frac{21497081974969\gamma_E}{555716700} + \frac{39542529067\pi^2}{3367980} \right. \\
& - \frac{15451532104941719 \log(2)}{27230118300} + \frac{34563425601321 \log(3)}{132809600} + \frac{3012745361328125 \log(5)}{34854551424} \left. \right) e^2 \\
& + \left(- \frac{671462220891497074433309}{160636640011848000} + \frac{26436888128127791\gamma_E}{12102274800} - \frac{3066363010741\pi^2}{10478160} \right. \\
& + \frac{1122122451633337997 \log(2)}{36306824400} - \frac{67683747020751 \log(3)}{75891200} - \frac{200964925537109375 \log(5)}{19916886528} \left. \right) e^4 \\
& + \left(- \frac{47316764670092138351403131}{680343416520768000} + \frac{1290798565697019809\gamma_E}{72613648800} - \frac{236118406034659\pi^2}{62868960} \right. \\
& - \frac{109330311453653376797 \log(2)}{217840946400} - \frac{126238870317372129 \log(3)}{772710400} + \frac{6190036871141024609375 \log(5)}{20076221620224} \\
& \left. + \frac{11717176456561231663 \log(7)}{292656291840} \right) e^6 + \dots + n_{18}e^{18} + \dots, \tag{6.33}
\end{aligned}$$

$$\begin{aligned}
\mathcal{L}_{8L^2} = & \frac{1}{(1-e^2)^{23/2}} \left(- \frac{20621469398683}{10892047320} - \frac{873082546975007}{15560067600} e^2 + \frac{8493235174147961}{48409099200} e^4 + \frac{1236049323927605309}{290454595200} e^6 \right. \\
& + \frac{28536838567917568709}{2323636761600} e^8 + \frac{2528975648094153077}{221298739200} e^{10} + \frac{3228304767170880073}{885194956800} e^{12} \\
& + \frac{4075229663605721917}{12392729395200} e^{14} + \frac{60344732583283}{16319643648} e^{16} \left. \right) + \frac{95}{2(1-e^2)^{10}} \left(\frac{366368}{11025} + \frac{189812971}{132300} e^2 + \frac{1052380631}{105840} e^4 \right. \\
& \left. + \frac{9707068997}{529200} e^6 + \frac{8409851501}{846720} e^8 + \frac{4574665481}{3386880} e^{10} + \frac{6308399}{301056} e^{12} \right), \tag{6.34}
\end{aligned}$$

$$\begin{aligned}
\mathcal{L}_{17/2} = & \frac{\pi}{(1-e^2)^{12}} \left[\frac{60050471374198816098730954501}{1083453442264445091840000} - \frac{16654515688953719\gamma_E}{2020034016000} - \frac{91049249\gamma_E^2}{132300} + \frac{91049249\pi^2}{529200} \right. \\
& - \frac{11256322928659829467 \log(2)}{381786429024000} - \frac{116527141\gamma_E \log(2)}{17150} - \frac{1632801787 \log^2(2)}{185220} - \frac{19606939404628941 \log(3)}{628455027200} \\
& + \frac{5544045\gamma_E \log(3)}{1372} + \frac{5544045 \log(2) \log(3)}{1372} + \frac{5544045 \log^2(3)}{2744} + \frac{49633544921875 \log(5)}{2544182784} - \frac{84807\zeta(3)}{70} + \\
& \left(- \frac{15036308338855532675849798486713}{6205233351150912798720000} + \frac{223778092210802539141\gamma_E}{104123571552000} - \frac{65904560053\gamma_E^2}{231525} + \frac{65904560053\pi^2}{926100} \right. \\
& + \frac{140869805086990295761 \log(2)}{163622755296000} + \frac{8623992122\gamma_E \log(2)}{33075} + \frac{310965709387 \log^2(2)}{231525} + \frac{12278674760615248437 \log(3)}{1571137568000} \\
& - \frac{1743776019\gamma_E \log(3)}{1715} - \frac{1743776019 \log(2) \log(3)}{1715} - \frac{1743776019 \log^2(3)}{3430} - \frac{13175186181640625 \log(5)}{4040068032} \\
& \left. - \frac{29942870443210501 \log(7)}{63604569600} + \frac{831792958\zeta(3)}{2205} \right) e^2 + \dots, \tag{6.35}
\end{aligned}$$

$$\begin{aligned}
\mathcal{L}_{17/2L} = & \frac{\pi}{(1-e^2)^{12}} \left[- \frac{16654515688953719}{4040068032000} - \frac{91049249\gamma_E}{132300} - \frac{116527141 \log(2)}{34300} + \frac{5544045 \log(3)}{2744} \right. \\
& + \left(\frac{223778092210802539141}{208247143104000} - \frac{65904560053\gamma_E}{231525} + \frac{4311996061 \log(2)}{33075} - \frac{1743776019 \log(3)}{3430} \right) e^2 \\
& + \left(\frac{1224651117880706056076827}{36651497186304000} - \frac{25340338934531\gamma_E}{3951360} - \frac{2672975873695021 \log(2)}{59270400} + \frac{33275639432241 \log(3)}{4390400} \right.
\end{aligned}$$

$$\begin{aligned}
& + \frac{25787353515625 \log(5)}{4741632} e^4 + \left(\frac{2447980141428133025519227}{10308233583648000} - \frac{19825641677397587 \gamma_E}{533433600} \right. \\
& \left. + \frac{335478276938768813 \log(2)}{533433600} + \frac{124568886652983 \log(3)}{4390400} - \frac{15233813134765625 \log(5)}{42674688} \right) e^6 + \dots + n_{16} e^{16} + \dots \Big], \tag{6.36}
\end{aligned}$$

$$\begin{aligned}
\mathcal{L}_{17/2L^2} = & \frac{\pi}{(1-e^2)^{12}} \left(-\frac{91049249}{529200} - \frac{65904560053}{926100} e^2 - \frac{25340338934531}{15805440} e^4 - \frac{19825641677397587}{2133734400} e^6 \right. \\
& - \frac{5146045059705234151}{273118003200} e^8 - \frac{49591538734543178399}{3413975040000} e^{10} - \frac{10634841767381874605891}{2621932830720000} e^{12} \\
& - \frac{126041444979520074540149}{385424126115840000} e^{14} - \frac{131123991469047848941021}{39467430514262016000} e^{16} + \frac{44427013734959710303}{285434095683502080000} e^{18} \\
& \left. + \frac{8359183360274467950273439}{25574894973241786368000000} e^{20} + \dots \right), \tag{6.37}
\end{aligned}$$

$$\begin{aligned}
\mathcal{L}_{9L^3} = & \frac{1}{(1-e^2)^{25/2}} \left(-\frac{313611008}{3472875} - \frac{105607281901}{10418625} e^2 - \frac{1882969493752}{10418625} e^4 - \frac{5247811027411}{5556600} e^6 - \frac{1237392658483}{694575} e^8 \right. \\
& \left. - \frac{81460556106397}{63504000} e^{10} - \frac{10573124400217}{31752000} e^{12} - \frac{599796978359}{24192000} e^{14} - \frac{89428139}{387072} e^{16} \right). \tag{6.38}
\end{aligned}$$

VII. CONCLUSIONS

As expected, the results in the energy flux at infinity closely mirror those of the angular momentum, with the terms $\mathcal{L}_2, \mathcal{L}_4, \mathcal{L}_{5L}, \mathcal{L}_6, \mathcal{L}_{6L}, \mathcal{L}_{7L}$, and \mathcal{L}_{8L^2} all repeating the trends noted in their \mathcal{J} counterparts. Overall, we have found new exact forms for five enhancement functions in each regime – $5L, 6L^2, 7L^2, 8L^2$, and $9L^3$ – with numerous more coefficients added to those terms with no closed forms. We immediately conclude that lmn fitting, along with the eulerlog simplification, is a viable method of extracting PN coefficients in the fluxes of eccentric-orbit EMRIs. Similar techniques should be possible in the conservative sector and could feasibly lead to improved expansions for certain quantities like the generalized redshift invariant [7, 17, 22].

Unfortunately, these methods do appear to reach some limitations around the 8PN integer series. After the eulerlog simplifications are performed, the 8PN integer term still requires that a search vector of length 5 be fit, $\{1, \pi^2, \pi^4, \zeta(3), 2\beta - \log(2)\}$. We find that such a search vector requires around 140–170+ decimals of accuracy to yield a correct result, depending on the fractional complexities involved. Maintaining that accuracy to such high order would necessitate flux calculations of 500 decimals or more. Worse, the 9PN non-log series would have a search vector length greater than 6, compounding these difficulties by an order of magnitude. Thus, even if we could increase the precision and obtain e coefficients in \mathcal{J}_8 , we see that the non-log series will become prohibitively expensive at 9PN and beyond.

However, many enhancement functions beyond the scope of this paper are still within reach. This possibility stems from the fact that each full PN order has some power or powers of log with a short search vector (possibly after simplification). The most fruitful have

the vector $\{1\}$, representing a rational series in e^2 . A coefficient in such a series only requires about $10 + f$ decimals of accuracy to extract for fractional complexity f . Length-2 search vectors are a little more cumbersome, but we find they still offer consistent results with moderate accuracy, say 70 or so decimals. Further still, even high-order terms with search vectors of length 3 will permit some measure of success. For example, despite almost no yield in \mathcal{J}_8 , two coefficients were found in $\mathcal{J}_{17/2}$, with vector $\{1, \pi^2, \zeta(3)\}$. Thus, it is these terms, with search vectors under length-4, which could be susceptible to the unmodified methods of this paper, feasibly to 12PN or beyond.

However, it would be more useful not to repeat these methods, but to improve them. Indeed, as briefly mentioned in Sec. IV the simplifications we have performed can be extended by utilizing eccentric-orbit analogs of the tail factorizations employed in [33]. Johnson-McDaniel relayed to us a MATHEMATICA notebook containing examples of an S_{lmn} factorization, with which all terms could be reduced to simple rational series until 8PN. This would likely allow for the computation of eccentricity coefficients across several more PN orders.

Furthermore, by also applying purely analytic expansions of the MST solutions, we will greatly enhance our ability to determine high PN contributions at lower orders in e^2 . Because the orbit-averaged fluxes compose the greatest contribution to the gravitational-wave phase [68, 69], and because accurate waveforms are sought in nearly all regions of parameter space (large and small y and e), expansions are required to very high PN order to simulate the range of possible EMRIs down to merger [13, 17]. These ideas will be explored fully in future work.

ACKNOWLEDGMENTS

We thank Nathan Johnson-McDaniel, Leor Barack, Luc Blanchet for helpful discussions. This work was supported in part by NSF grants PHY-1506182 and PHY-1806447. C.R.E. acknowledges support from the Bahnsen Fund at the University of North Carolina-Chapel Hill. This work was also supported by the North Carolina Space Grant.

Appendix A: Flux expansions using the semi-latus rectum

Although we have chosen to follow the PN convention of using $y = (M\Omega_\varphi)^{2/3}$ as our expansion parameter, in some ways this is not the most natural variable to use. To see this, consider the flux expression including only the lowest-order enhancement factor,

$$\begin{aligned} \left\langle \frac{dE}{dt} \right\rangle_{0\text{PN}} &= \frac{32}{5} \left(\frac{\mu}{M} \right)^2 \\ &\times \frac{y^5}{(1-e^2)^{7/2}} \left(1 + \frac{73}{24} e^2 + \frac{37}{96} e^4 \right). \end{aligned} \quad (\text{A1})$$

Note that at this order the eccentricities e and e_t are equivalent. The primary drawback of this expression is the singular factor $(1-e^2)^{-7/2}$, which causes the flux to diverge as $e \rightarrow 1$. This factor can be traced back to the choice of x as a PN variable. However, we may choose to write x as an expansion in p^{-1} , which to leading order goes as

$$y = (1-e^2)/p + \mathcal{O}(p^{-2}). \quad (\text{A2})$$

Re-expressed as an expansion in $1/p$, the 0PN flux is then

$$\begin{aligned} \left\langle \frac{dE}{dt} \right\rangle_{0\text{PN}} &= \frac{32}{5} \left(\frac{\mu}{M} \right)^2 \\ &\times \frac{(1-e^2)^{3/2}}{p^5} \left(1 + \frac{73}{24} e^2 + \frac{37}{96} e^4 \right). \end{aligned} \quad (\text{A3})$$

In this expression, the flux no longer diverges as $e \rightarrow 1$, but instead it goes to zero, which is also not ideal.

Far more useful is to compute not the flux, but rather the total energy radiated during one radial libration. We find this by multiplying the flux by the radial period. Expanded in p^{-1} , the radial period carries a factor of $(1-e^2)^{-3/2}$ which exactly cancels the offending term in Eqn. (A3), leaving

$$T_r \left\langle \frac{dE}{dt} \right\rangle_{0\text{PN}} = \frac{64\pi}{5} \frac{\mu^2}{M} \frac{1}{p^{7/2}} \left(1 + \frac{73}{24} e^2 + \frac{37}{96} e^4 \right). \quad (\text{A4})$$

Thus, for a given PN order, the energy radiated is finite and nonzero in the limit $e \rightarrow 1$.

The total energy radiated in one radial period can be written in a form reminiscent of Eqn. (6.1)

$$T_r \left\langle \frac{dE}{dt} \right\rangle = \frac{64\pi}{5} \frac{\mu^2}{M} \frac{1}{p^{7/2}} \left(\bar{\mathcal{L}}_0 + \frac{\bar{\mathcal{L}}_1}{p^1} + \frac{\bar{\mathcal{L}}_{3/2}}{p^{3/2}} + \dots \right), \quad (\text{A5})$$

with further terms coming every half-order in p . Through 2.5PN the \mathcal{L} terms are

$$\bar{\mathcal{L}}_0 = 1 + \frac{73}{24} e^2 + \frac{37}{96} e^4 \quad (\text{A6})$$

$$\bar{\mathcal{L}}_1 = -\frac{239}{336} - \frac{5065}{672} e^2 - \frac{211}{128} e^4 + \frac{2393}{5376} e^6 \quad (\text{A7})$$

$$\begin{aligned} \bar{\mathcal{L}}_{3/2} &= 4\pi + \frac{1375\pi}{48} e^2 + \frac{3935\pi}{192} e^4 + \frac{10007\pi}{9216} e^6 \\ &\quad + \frac{2321\pi}{221184} e^8 - \frac{237857\pi}{88473600} e^{10} + \dots \end{aligned} \quad (\text{A8})$$

$$\begin{aligned} \bar{\mathcal{L}}_2 &= -\frac{11623}{4536} - \frac{328673}{4536} e^2 - \frac{18668}{189} e^4 \\ &\quad - \frac{20477}{2016} e^6 + \frac{61703}{64512} e^8 \end{aligned} \quad (\text{A9})$$

$$\begin{aligned} \bar{\mathcal{L}}_{5/2} &= -\frac{127\pi}{672} - \frac{2461\pi}{42} e^2 - \frac{5363069\pi}{43008} e^4 - \frac{6867607\pi}{387072} e^6 \\ &\quad + \frac{9437735\pi}{7077888} e^8 + \frac{10400743\pi}{123863040} e^{10} + \dots \end{aligned} \quad (\text{A10})$$

Note in particular that at 2PN the two separate singular pieces $[(1-e^2)^{11/2}$ and $(1-e^2)^4]$ combine to form one nonsingular term. The 1.5PN and 2.5PN terms are still not closed form, although they too are nonsingular

- [1] L. Barack, V. Cardoso, S. Nissanke, T. P. Sotiriou, and *et al.*, *Classical and Quantum Gravity* **36**, 143001 (2019), arXiv:1806.05195 [gr-qc].
- [2] P. Amaro-Seoane, J. R. Gair, M. Freitag, M. C. Miller, I. Mandel, C. J. Cutler, and S. Babak, *Classical and Quantum Gravity* **24**, R113 (2007), astro-ph/0703495.
- [3] “elisa science home page,” <http://www.elisascience.org/>.
- [4] “Lisa home page,” <http://sci.esa.int/lisa/>.
- [5] E. Poisson, A. Pound, and I. Vega, *Living Rev. Rel.* **14**, 7 (2011), arXiv:gr-qc/1102.0529.
- [6] L. Blanchet, *Living Reviews in Relativity* **17**, 2 (2014), arXiv:1310.1528 [gr-qc].
- [7] S. Detweiler, *Phys. Rev. D* **77**, 124026 (2008), arXiv:0804.3529 [gr-qc].
- [8] N. Sago, L. Barack, and S. L. Detweiler, *Phys. Rev. D* **78**, 124024 (2008), arXiv:0810.2530 [gr-qc].
- [9] L. Barack and N. Sago, *Physical Review Letters* **102**, 191101 (2009), arXiv:0902.0573 [gr-qc].
- [10] L. Blanchet, S. Detweiler, A. Le Tiec, and B. F. Whiting, *Phys. Rev. D* **81**, 064004 (2010), arXiv:0910.0207 [gr-qc].
- [11] L. Blanchet, S. Detweiler, A. Le Tiec, and B. F. Whiting, *Phys. Rev. D* **81**, 084033 (2010), arXiv:1002.0726 [gr-qc].
- [12] R. Fujita, *Progress of Theoretical Physics* **127**, 583 (2012), arXiv:1104.5615 [gr-qc].
- [13] R. Fujita, *Progress of Theoretical Physics* **128**, 971 (2012), arXiv:1211.5535 [gr-qc].
- [14] A. G. Shah, J. L. Friedman, and B. F. Whiting, *Phys. Rev. D* **89**, 064042 (2014), arXiv:1312.1952 [gr-qc].
- [15] A. G. Shah, *Phys. Rev. D* **90**, 044025 (2014), arXiv:1403.2697 [gr-qc].
- [16] S. R. Dolan, P. Nolan, A. C. Ottewill, N. Warburton, and B. Wardell, *Phys. Rev. D* **91**, 023009 (2015), arXiv:1406.4890 [gr-qc].
- [17] N. K. Johnson-McDaniel, A. G. Shah, and B. F. Whiting, *Phys. Rev. D* **92**, 044007 (2015), arXiv:1503.02638 [gr-qc].
- [18] D. Bini, T. Damour, and A. Gericco, (2015), arXiv:1511.04533 [gr-qc].
- [19] S. Akcay, A. Le Tiec, L. Barack, N. Sago, and N. Warburton, *Phys. Rev. D* **91**, 124014 (2015), arXiv:1503.01374 [gr-qc].
- [20] N. Sago and R. Fujita, *Progress of Theoretical and Experimental Physics* **2015**, 073E03 (2015), arXiv:1505.01600 [gr-qc].
- [21] E. Forseth, C. R. Evans, and S. Hopper, *Phys. Rev. D* **93**, 064058 (2016).
- [22] S. Hopper, C. Kavanagh, and A. C. Ottewill, *Phys. Rev. D* **93**, 044010 (2016), arXiv:1512.01556 [gr-qc].
- [23] D. Bini, T. Damour, and A. Gericco, *Physical Review D* **93**, 064023 (2016), arXiv:1511.04533 [gr-qc].
- [24] D. Bini, T. Damour, and A. Gericco, *Physical Review D* **93**, 104017 (2016), arXiv:1601.02988 [gr-qc].
- [25] D. Bini, T. Damour, and A. Gericco, *Physical Review D* **93**, 124058 (2016), arXiv:1602.08282 [gr-qc].
- [26] C. Munna and C. R. Evans, *Phys. Rev. D* **100**, 104060 (2019), arXiv:1909.05877 [gr-qc].
- [27] S. Mano, H. Suzuki, and E. Takasugi, *Progress of Theoretical Physics* **96**, 549 (1996), gr-qc/9605057.
- [28] S. Mano, H. Suzuki, and E. Takasugi, *Progress of Theoretical Physics* **95**, 1079 (1996), gr-qc/9603020.
- [29] K. Ganz, W. Hikida, H. Nakano, N. Sago, and T. Tanaka, *Progress of Theoretical Physics* **117**, 1041 (2007), gr-qc/0702054.
- [30] R. Fujita, *Prog. Theor. Exp. Phys.* **2015** (2015), 10.1093/ptep/ptv012, arXiv:1412.5689 [gr-qc].
- [31] S. Hopper, E. Forseth, T. Osburn, and C. R. Evans, *Phys. Rev. D* **92**, 044048 (2015), arXiv:1506.04742 [gr-qc].
- [32] H. R. P. Ferguson, D. H. Bailey, and S. Arno, *Journal of Mathematics of Computation* **68**, 351 (1999).
- [33] N. K. Johnson-McDaniel, *Phys. Rev. D* **90**, 024043 (2014), arXiv:1405.1572 [gr-qc].
- [34] C. Munna and C. R. Evans, to be submitted to *Phys. Rev. D*.
- [35] K. G. Arun, L. Blanchet, B. R. Iyer, and S. Sinha, *Phys. Rev. D* **80**, 124018 (2009), arXiv:0908.3854 [gr-qc].
- [36] K. G. Arun, L. Blanchet, B. R. Iyer, and M. S. S. Quisailah, *Phys. Rev. D* **77**, 064034 (2008), arXiv:0711.0250 [gr-qc].
- [37] K. G. Arun, L. Blanchet, B. R. Iyer, and M. S. S. Quisailah, *Phys. Rev. D* **77**, 064035 (2008), arXiv:0711.0302 [gr-qc].
- [38] T. Damour, B. Iyer, and A. Nagar, *Phys. Rev. D* **79**, 064004 (2009), arXiv:0811.2069 [gr-qc].
- [39] E. R. Forseth, *High-precision extreme-mass-ratio inspirals in black hole perturbation theory and post-Newtonian theory*, Ph.D. thesis, The University of North Carolina at Chapel Hill (2016).
- [40] “Black Hole Perturbation Toolkit,” bhptoolkit.org.
- [41] K. Martel and E. Poisson, *Phys. Rev. D* **71**, 104003 (2005), arXiv:gr-qc/0502028.
- [42] M. Sasaki and H. Tagoshi, *Living Reviews in Relativity* **6**, 6 (2003), gr-qc/0306120.
- [43] C. Darwin, *Proceedings of the Royal Society of London Series A* **263**, 39 (1961).
- [44] C. Cutler, D. Kennefick, and E. Poisson, *Phys. Rev. D* **50**, 3816 (1994).
- [45] L. Barack and N. Sago, *Phys. Rev. D* **81**, 084021 (2010), arXiv:1002.2386 [gr-qc].
- [46] I. S. Gradshteyn, I. M. Ryzhik, A. Jeffrey, and D. Zwillinger, *Table of Integrals, Series, and Products, Seventh Edition Elsevier Academic Press, 2007. ISBN 012-373637-4* (2007).
- [47] K. Martel, *Phys. Rev. D* **69**, 044025 (2004).
- [48] S. Chandrasekhar, *Royal Society of London Proceedings Series A* **343**, 289 (1975).
- [49] S. Chandrasekhar and S. Detweiler, *Royal Society of London Proceedings Series A* **345**, 145 (1975).
- [50] S. Chandrasekhar, *The Mathematical Theory of Black Holes*, The International Series of Monographs on Physics, Vol. 69 (Clarendon, Oxford, 1983).
- [51] M. Berndston, *Harmonic Gauge Perturbations of the Schwarzschild Metric*, Ph.D. thesis, University of Colorado (2007), arXiv:0904.0033v1.
- [52] J. M. Bardeen and W. H. Press, *Journal of Mathematical Physics* **14**, 7 (1973).
- [53] S. Hopper and C. R. Evans, *Phys. Rev. D* **82**, 084010 (2010).
- [54] L. Barack, A. Ori, and N. Sago, *Phys. Rev. D* **78**, 084021 (2008), arXiv:0808.2315.
- [55] L. Blanchet and G. Schäfer, *Classical and Quantum*

- Gravity **10**, 2699 (1993).
- [56] R. Rieth and G. Schäfer, *Classical and Quantum Gravity* **14**, 2357 (1997).
- [57] P. C. Peters, *Physical Review* **136**, 1224 (1964).
- [58] N. Loutrel and N. Yunes, *Classical and Quantum Gravity* **34**, 044003 (2017), arXiv:1607.05409 [gr-qc].
- [59] DLMF, “NIST Digital Library of Mathematical Functions,” <http://dlmf.nist.gov/>, Release 1.0.10 of 2015-08-07, online companion to [70].
- [60] D. Bini and T. Damour, *Phys. Rev.* **D87**, 121501 (2013), arXiv:1305.4884 [gr-qc].
- [61] D. Bini and T. Damour, *Phys. Rev. D* **89**, 064063 (2014), arXiv:1312.2503 [gr-qc].
- [62] D. Bini and T. Damour, *Phys. Rev.* **D90**, 024039 (2014), arXiv:1404.2747 [gr-qc].
- [63] D. Bini and T. Damour, *Phys. Rev.* **D90**, 124037 (2014), arXiv:1409.6933 [gr-qc].
- [64] C. Kavanagh, A. C. Ottewill, and B. Wardell, *Phys. Rev. D* **92**, 084025 (2015), arXiv:1503.02334 [gr-qc].
- [65] Munna, Christopher, to be submitted to *Phys. Rev. D*.
- [66] A. Granville, *Algorithmic Number Theory: Lattices, Number Fields, Curves and Cryptography*, edited by J. P. Buhler and P. Stevenhagen, Mathematical Sciences Research Institute Publications, Vol. 44 (Cambridge University Press, New York, NY, 2008).
- [67] W. Goldberger and A. Ross, *Phys. Rev. D* **81**, 124015 (2010).
- [68] T. Hinderer and E. E. Flanagan, *Phys. Rev. D* **78**, 064028 (2008), arXiv:0805.3337 [gr-qc].
- [69] E. E. Flanagan and T. Hinderer, *Physical Review Letters* **109**, 071102 (2012), arXiv:1009.4923 [gr-qc].
- [70] F. W. J. Olver, D. W. Lozier, R. F. Boisvert, and C. W. Clark, eds., *NIST Handbook of Mathematical Functions* (Cambridge University Press, New York, NY, 2010) print companion to [59].